# Annual analysis of the photovoltaic direct-expansion heat pump assisted by double condensing equipment for secondary power generation

Zhiying Song[a,b,c], Jie Ji[a,b]*, Yuzhe Zhang[a,b], Yunhai Li[c], Jing Li[c], Xudong Zhao[c]

[a]*Department of Thermal Science and Energy Engineering, University of Science and Technology of China, Hefei 230026, China*

[b]*Key Laboratory of Solar Thermal Conversion of Anhui Province, Hefei, 230026, Anhui, China.*

[c]*Centre for Sustainable Technology, University of Hull, Hull, HU6 7RX, UK*

* Corresponding author. E-mail address: jijie@ustc.edu.cn

**Abstract**: Thermoelectric generation (TEG) converts heat directly into electricity based on temperature difference. Many studies on combining TEG with photovoltaics to convert waste heat into electricity to increase overall power generation have been conducted. However, through previous research, if TEG was installed between the cooling and PV, it will hinder PV heat dissipation and cause electricity deterioration, which could not be compensated by TEG output. To ensure the PV cooling and meanwhile realize thermoelectric conversion, a photovoltaic direct-expansion double-condensing heat pump system based on TEG assisted by micro-channel heat pipes and water-cooling condenser is proposed. Experiments & mathematical model are carried out & verified. The regional weather conditions at different latitudes and altitudes are adopted to predict the system performance on a year basis. From the results, the electrical efficiency is improved due to the additional TEG power output. With a higher ambient temperature in Hongkong, the heating capacity is higher, but the compressor consumption also increases. With better irradiation and a lower ambient temperature, Garze has brilliant electrical performance, the $COP_{PVT}$ & NEER are the highest at 9.9 monthly & 8.0 annually. Furthermore, the operating costs and $CO_2$ emissions of this system are just 1/4~1/3 and 1/3~1/2 of gas boiler, indicating significant potential for energy-savings & emission reduction.

**Keywords:** Annual analysis; Direct-expansion solar-assisted heat pump; Micro-channel heat pipe; Thermoelectric generator; Double condensing

***Nomenclature***

| | | | |
|---|---|---|---|
| $A$ | area, $m^2$ | $\eta$ | efficiency |
| C | circumference, m | ***Abbreviation*** | |
| $c_p$ | specific heat capacity, $J \cdot kg^{-1} \cdot K^{-1}$ | COP | coefficient of performance |
| | | DX | direct expansion |

| | | | |
|---|---|---|---|
| $Ex$ | exergy, J | NEER | net energy efficiency ratio |
| $D$ | diameter, m | MCHP | micro-channel heat pipe |
| $k$ | conduction coefficient, $W \cdot m^{-1} \cdot K^{-1}$ | TEG | thermoelectric generator |
| $K$ | heat transfer coefficient, $W \cdot m^{-2} \cdot K^{-1}$ | SAHP | solar assisted heat pump |
| $I$ | current, A | PV | photovoltaic |
| $h$ | specific enthalpy, $J \cdot kg^{-1}$ | PVT | photovoltaic and thermal |
| $G$ | irradiation, $W \cdot m^{-2}$ | ***Subscripts*** | |
| $l$ | Weld width/Length, m | a | ambient |
| $R_t$ | total thermal resistance, $K \cdot W^{-1}$ | be | Absorber board in evaporator |
| $R$ | total electrical internal resistance, Ω | bc | absorber board in condenser |
| $\dot{Q}$ | heat flux, W | cov | convection |
| $P$ | power, W | com | compressor |
| $\dot{m}$ | mass flow rate, $kg \cdot s^{-1}$ | ol | outlet |
| $T$ | temperature, K | out | outside |
| $t$ | time, s | low | low-temperature end of the TEG |
| $S$ | total Seebeck coefficient, $V \cdot K^{-1}$ | high | high-temperature end of the TEG |
| $u$ | speed, $m \cdot s^{-1}$ | j | thermal silica |
| $x$ | dryness | il | inlet |
| | | in | inside |
| ***Greek symbols*** | | ref | refrigerant |
| $\varepsilon$ | emissivity | rad | radiation |
| $\rho$ | density, $kg \cdot m^{-3}$ | pc | condensing pipeline |
| $\kappa$ | coverage | pe | evaporating pipeline |
| $\varphi$ | temperature influence coefficient, $K^{-1}$ | wt | water tank |
| $\beta$ | conversion efficiency | wc | water channel |

| | | | |
|---|---|---|---|
| $\delta$ | thickness, m | w | water |
| $\alpha$ | absorptivity | th | thermal |

## 1.Introduction

Global warming is a very urgent situation that the world is currently exposed to and people need to handle it. Global warming would increase the potential of local flooding, raise the sea level, disturb the balance of nature, and bring multiple risks to humans and other creatures on earth. Therefore, it is of great importance to slow down the deterioration of global warming by restricting the usage of fossil fuels, switching to cleaner renewable energy, and improving the energy efficiency. In a state of rapid development, especially supported by manufacturing, China has a huge demand for energy and could generate a large amount of greenhouse gases every year[1]. Although China has announced to realize carbon peaking by 2030 & carbon neutrality by 2060[2], it is still a hard goal.

Heat pump (HP) system is proven to be a high efficient, energy-saving, and emission-reduction device to support heat[3] in contrast to a gas-heating device, which occupies a large amount of the market nowadays. By inputting a small amount of mechanical energy, the heat pump system could transfer a large amount of heat to a high-temperature source from a low-temperature environment[4] to realize high efficient heating. Energy consumption and carbon emissions of buildings are responsible for 46% and 50% of the total amount in China [5]. Thus, the heat pump system is valuable to improve the energy structure of China. Featuring inexhaustibility and wide distribution[6], solar energy stands out among the various sustainable energies[7]. By putting the solar energy and HP together, the solar-assisted heat pump (SAHP) system could fully utilize solar energy as well as enhance the performance of heat pumps[8], which is attractive to researchers. Wang [9] proposed a HP system adopting solar and air sources to provide multifunction: space heating, domestic water heating, and combined heating and cooling. The switch logic was established to cope with the inconsistent and variable nature of solar energy and the mean COPs for space heating and domestic hot water were 4.25 and 3.94, respectively, providing better performance compared with traditional air-source heat pump. Considering the increased space-heating load resulting from the accompanied secondary space cooling in heat pump water heater, Treichel[10] constructed a heat pump system with air-based solar thermal collectors to reduce the heating/cooling load. Jiang [11] created a novel triangular solar air collector to help the air-source heat pump system perform better based on previous paper[12]. The system could provide ventilation, defrosting, and heating through parallel, preheating, and series operation. An increase of 64.4% of the system's COP was realized under the optimal operation modes according to the modified boundary equations. Fan [13] proposed a heat recovery air-source heat pump combined with multiple-throughout-flow micro-channel solar thermal panels array that functioned as solar-assisted heating

device. The compound heat pump system could collect heat from the indoor/outdoor air as well as from irradiation. Experimental results showed that solar efficiency was lifted by 8-15% while COP was enhanced by 30%. Lee [14] used solar heat collectors to assist the ground-source HP system to realize energy-saving while supplying heat. The series and parallel modes were all analyzed, and it was found that the parallel layout was better for heating-dominated areas. Besides, the comparative investigation on $CO_2$ emissions and life cycle performance was conducted by using low-GWP refrigerants[15].

Among those SAHP systems, the photovoltaic direct-expansion heat pumps (PV-DXHP) present excellent system performance due to their unique PV-cooling evaporator[16]. In comparison to traditional PVT systems using water cooling, PV cells in the PV-DXHP system show a much lower operating temperature[17]. Thus, studies on PV-DXHP systems are flourishing. Abbas [18] employed PV/T evaporators to a DXHP system to realize high electricity and heat generation simultaneously. According to the experimental and numerical study, the mean thermal efficiency, electrical efficiency, and COP were 66.71%, 14.08%, and 6.11. Song[19] applied different concentrated PV evaporators to a DXHP system and carried out performance comparison studies. The Fresnel concentration system showed the best capacities. Yao [20] applied the roll-bond panel below the PV plate to act as the refrigerant channel in the heat pump cycle. Benefiting from better contact, the heat exchange between the PV and the refrigerant was improved, resulting in a more even PV temperature distribution. Then the PVT heat pump system was compared with the PV system[21], and it was found that the system with average electrical and thermal efficiencies of 17.93% and 109.4%, could fix 53.2% more carbon emissions than that of the PV system after 20 years per $m^2$. The PV-SAHP system used as a water heater was also built by Ji[16], and the mathematical investigation under different climatic conditions, such as Tibet[22] & Hongkong[23], was also completed.

Aside from other energy-utilization technologies, the thermoelectric generator (TEG), which converts heat directly into electricity based on temperature difference[24], is widely used in solar-electric systems. For example, Zhang[25] got electricity output from the solar heat by applying TEG to the concentrated PV/T system. Under the PV panel, Shittu[26] applied micro-channel heat pipe (MCHP) and then installed TEG to the condensing section to transform the solar heat on PV into electricity. Wen[27] added a liner Fresnel lens to the PV/TEG system similar to Shittu's work but found that with a higher temperature gradient of TEG between the cooling fluid and PV, its total electrical efficiency declined, meaning that the inappropriate design of TEG may have negative effects.

TEG was proposed to be installed between concentrated PV (high temperature) and the evaporator (low temperature) in the initial exploratory research [28, 29]. But by comparison in the later work [19], it was exposed that TEG could increase the heat resistance between the PV and evaporator, resulting in a higher PV temperature. The power generation of TEG could not compensate for the detriment of PV electricity. To produce additional electricity by utilizing the thermoelectric effect and

simultaneously eliminate its hindrance to PV cooling in PV-DXHP system, the TEG is proposed to be installed in the condenser section[30]. Moreover, the MCHP is also constructed, because a larger temperature gap is beneficial for higher TEG conversion efficiency[31]. In this paper, the photovoltaic direct-expansion dual-condensing heat pump system based on TEG assisted by micro-channel heat pipes (MCHP/TEG) and water-cooling condenser (PV-DC-SAHP) is established. Experiments have been carried out. The mathematical model is completed and validated by experimental data. The annual performance of the system under different climatic conditions is investigated and compared. Besides, the carbon emissions and heating costs of the proposed system and traditional gas boiler are calculated and compared.

## 2. System presentation

In this part, the structure of the photovoltaic direct-expansion heat pump system featuring double-condensing equipment (PV-DC-SAHP) is presented in detail. The two condensing parts: 1.the refrigerant coil in a water tank; 2.the TEG condenser assisted by MCHP and water flowing (MCHP/TEG condenser). Fig.1 illustrates the layout of the MCHP/TEG condenser. All the heat exchange structures are insulated and encapsulated. The condensing refrigerant in MCHP/TEG condenser flows through two kinds of pipes: the 10mm-diameter branch pipes and the 19mm-diameter collecting pipes. There are 22 branch pipes connecting the collecting pipes, and only two diagonally symmetrical orifices of the two collecting pipes are open. The condensing refrigerant enters the collecting pipe, passes through the branch pipes, and then converges in the other collecting pipe to flow out. Thermal silica is used to glue the 16 MCHPs below the absorber plate. On the upper surface of the plate, the refrigerant pipes are laser-welded for better heat transfer. The glued evaporating section of the 16 MCHPs obtains heat from high-temperature refrigerant and releases it to the condensing section where the corresponding 16 TEGs are glued. Under the TEGs is the water channel with cooling water inside. The MCHP is 1940mm long and 60mm wide. The TEG has a square surface with a side length of 55mm. The length of the water channel is 960mm, and the cross section is a square with a side length of 60mm. In the system, there are two cycles: one is the refrigerant cycle, and the other is the water flow cycle. The water flows out from the water tank bottom and enters the water channel to take away the unconverted heat from TEG, and at last, the water carrying heat comes back to the tank. More detailed parameters of the test rig are listed in Table 2.

The experiment device is depicted in Fig. 2, and the detailed connection and measurement diagram is depicted in Fig. 3. Four PV plates in a shunt connection with copper pipes welded below are the evaporating part. The PV cells occupy 90.26% of the entire PV plate, whose width is 980mm and length is 1000mm. The rest of the surface area is black TPT material, whose absorption coefficient is high at 0.98. A Hitachi SD145CV-H6A compressor is used in the test, and the capillary is 2m long. During the test, 300L water is heated in the tank by the coil condenser, whose temperature is defined

as the mean value of the 5 temperature sensors that are vertically equidistantly inserted in the tank. Refrigerant temperatures, water temperatures, and refrigerant pressures are collected by thermocouples and pressure sensors, whose locations are illustrated in Fig.3. Apart from that, the irradiance and wind velocity are also collected by an irradiance meter and a wind speed sensor, while MPPT is used to control the PV output and charge the battery. The detailed information on the measuring and data collection devices is listed in Table.1.

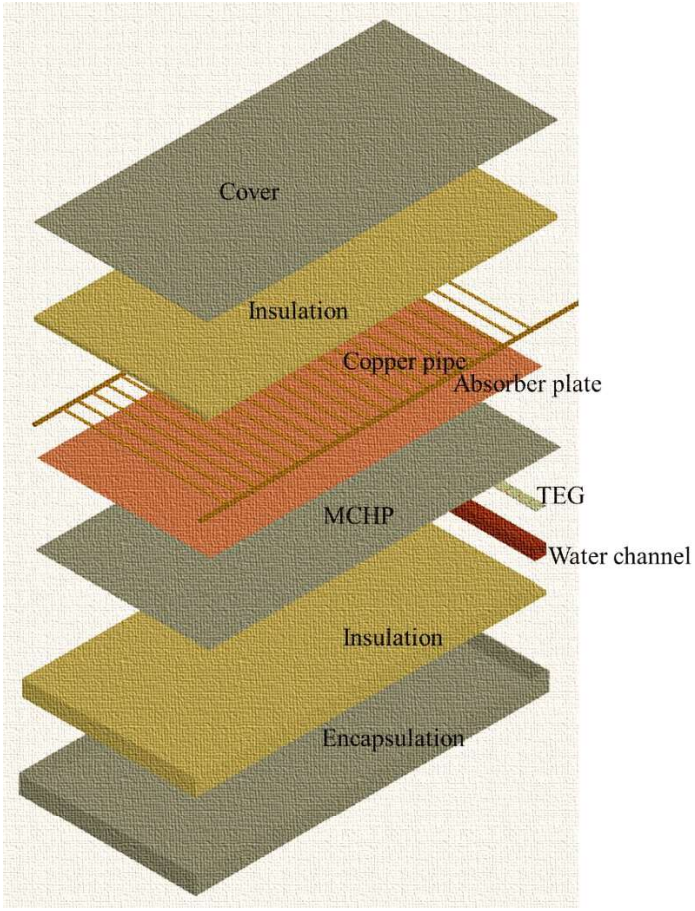


Fig.1 The layout of MCHP/TEG condenser

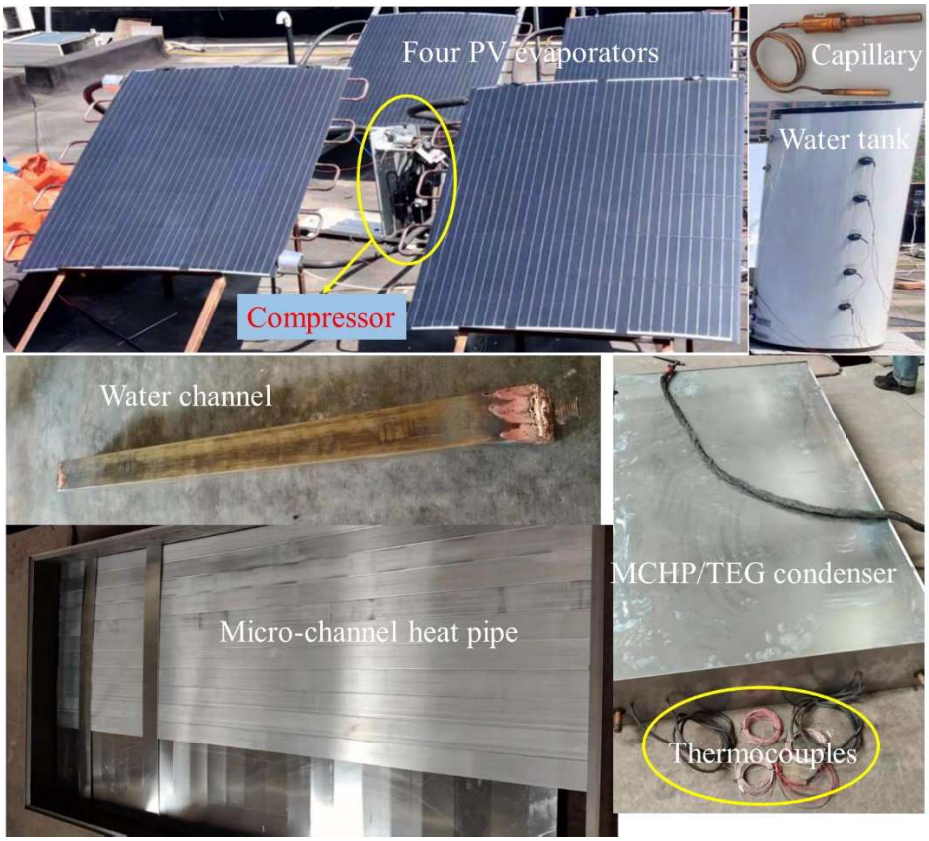


Fig.2 Test rig of the compound system

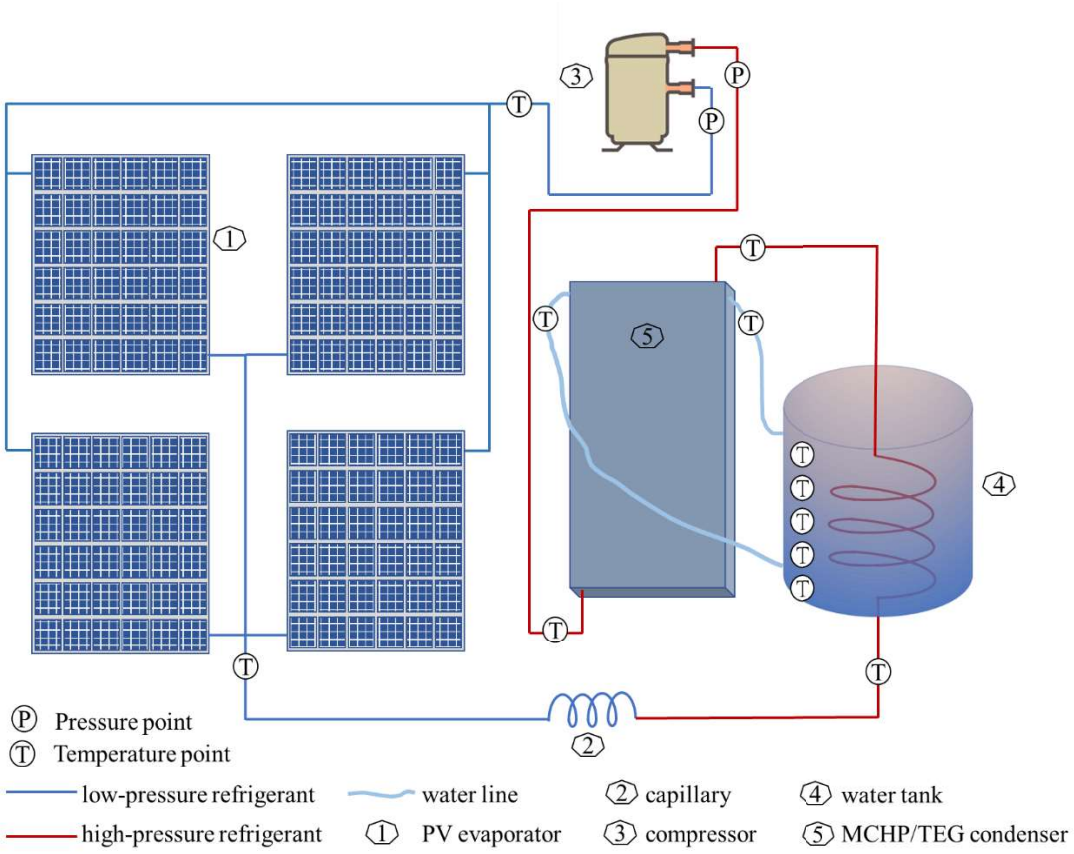


Fig.3 The diagram of the proposed system

149 Table.1 The parameters of the testing instruments

| Testing instrument | Technical parameter | Testing accuracy |
|---|---|---|
| Portable data acquisition instrument | HIOKI LR8400-21 | - |
| MPPT | Voltage:24V/36V/48V, Current:0-40A | - |
| T-type thermocouple | Range: -100□-100□ | ±0.2□ |
| Pressure sensor | PTS570, Range: 0-25bar | 0.3% |
| Irradiance meter | TBQ-2, Range: 0-2000W/m$^2$ | <2% |
| Wind speed sensor | RS-FSJT-V10, Range: 0-30m/s | ±0.2m/s |
| Power sensor | YOKOGAWA WT230, Range:0–12 kW | 0.5% |

150

151 Table.2 Parameters of the test rig

| Component | Parameters | Value |
|---|---|---|
| PV evaporator | Surface area of absorber plate | 980*1000 mm$^2$ |
| | Surface area of PV cells | 156.75*156.75 mm$^2$ |
| | Number of PV cells | 36 |
| | Temperature influence coefficient of PV | 0.0045 K$^{-1}$ |
| | PV efficiency at reference temperature | 0.19 |
| | Absorptivity of PV cell | 0.9 |
| | Thickness of the PV | 0.4 mm |
| | Thickness of the absorber board | 1.16 mm |
| | Evaporation pipe outer diameter | 10 mm |
| | Evaporation pipe inner diameter | 9.5 mm |
| MCHP/TEG Condenser | Thickness of the square copper tube | 2 mm |
| | Branch pipes outer diameter | 10 mm |
| | Branch pipes inner diameter | 9.5 mm |
| | Collecting pipes outer diameter | 19 mm |
| | Collecting pipes inner diameter | 18.4 mm |
| | Thermal conductivity of the absorbing board | 238 J·m$^{-2}$·K$^{-1}$ |
| | Thermal conductivity of the MCHP | 23000 W·m$^{-1}$·K$^{-1}$ |
| | Specific heat capacity of the absorbing board | 917 J·kg$^{-1}$·K$^{-1}$ |
| | Length of the MCHP | 1.94 m |
| | Width of MCHP | 60 mm |
| | Number of MCHP | 16 |
| Water tank condenser | Volume | 300 L |
| | Refrigerant pipe inner diameter | 8.53 mm |
| | Refrigerant pipe outer diameter | 9.01 mm |
| Capillary | Inner diameter | 1.2 mm |
| | Length | 2 m |
| Compressor | Rotating speed | 50 rad/s |
| | Displacement | 1.54*10$^{-5}$ m$^3$ |

152

153 # 3. Modeling

154 ## 3.1 Evaporating section

155 The evaporating section is mainly composed of the PV plate, the absorber plate, and the evaporating

pipe.

In the PV layer, the PV cells absorb irradiation, part of which is converted into electricity, while the rest is transformed into heat, participating in the heat calculation. Apart from the solar heat, PV cells also exchange heat with the air convectively, with the sky radiatively, and with the evaporating board (absorber board) conductively:

$$\kappa\rho_{pv}c_{p,pv}\frac{dT_{pv}}{dt}=k_{pv}\frac{\partial^2 T_{pv}}{\partial x^2}+k_{pv}\frac{\partial^2 T_{pv}}{\partial y^2}+\frac{\kappa}{\delta_{pv}}\left(G\alpha_{pv}\left(1-\beta\left(1-\varphi\left(T_{pv}-298.15\right)\right)\right)+K_{\cos}\left(T_a-T_{pv}\right)+K_{rad}\left(T_{sky}-T_{pv}\right)+K_{pv-be}\left(T_{be}-T_{pv}\right)\right) \quad (1)$$

$\kappa$ is the PV coverage of the PV layer; $\alpha$, $\beta$, and $\varphi$ are the absorptivity, standard photovoltaic conversion efficiency, and temperature influence coefficient of PV cells; $K_{\cos}$, $K_{rad}$, and $K_{pv-be}$ are the heat transfer coefficients between PV cells and the air, PV cells and the sky, PV cells and the evaporating board.

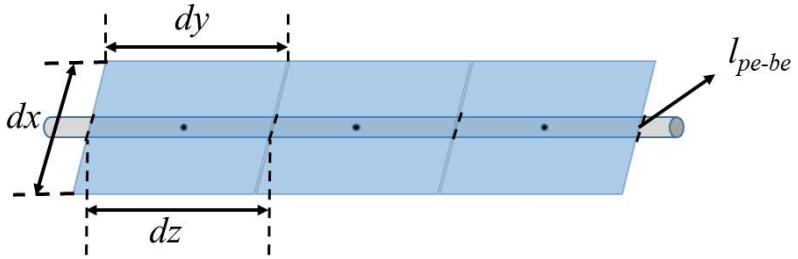


Fig.4 The meshing of the calculated volume

In the surface area covered by the PV cells, the absorber board exchanges heat with the PV. In the surface area without PV cells and filled with TPT material, the irradiation is collected. On the lower surface of the plate, the area in contact with the welded pipe has heat conduction, while the rest part will exchange heat with the air. The meshing in Fig.4 could help to understand the equation.

$$\rho_{be}c_{p,be}\frac{\partial T_{be}}{\partial t}=k_{be}\frac{\partial^2 T_{be}}{\partial y^2}+k_{be}\frac{\partial^2 T_{be}}{\partial x^2}+\frac{1}{\delta_{be}}\left(\kappa\left(T_{pv}-T_{be}\right)K_{pv-be}+\left(1-\kappa\right)G\alpha_{TPT}+\frac{K_{pe-be}l_{pe-be}\left(T_{pe}-T_{be}\right)}{dx}+(1-\frac{l_{pe-be}}{dx})K_{a-be}\left(T_a-T_{be}\right)\right) \quad (2)$$

$\alpha_{TPT}$ is the radiation absorptivity of TPT; $l_{pe-be}$ is the welding width; $K_{pe-be}$ and $K_{a-be}$ are the heat transfer coefficients between the evaporating pipe and the evaporating board, the air and the evaporating board.

The evaporating pipe would exchange heat with the inner flowing refrigerant and the absorber board:

$$\rho_{pe}c_{p,pe}\frac{\partial T_{pe}}{\partial t}=k_{pe}\frac{\partial^2 T_{pe}}{\partial z^2}+\frac{4}{\pi\left(D_{pe,out}^2-D_{pe,in}^2\right)}\left(\pi D_{pe,in}K_{ref-pe}\left(T_{ref}-T_{pe}\right)+K_{pe-be}l_{pe-be}\left(T_{be}-T_{pe}\right)\right) \quad (3)$$

$K_{ref-pe}$ is the heat exchange coefficient between the evaporating pipe and the refrigerant; $T_{ref}$ is the refrigerant temperature.

### 3.2 Double-condensing section

The double-condensing section has two parts:

***The MCHP/TEG part***

In the MCHP/TEG condenser, the condensing pipe collects heat from the high-temperature refrigerant and conducts the heat to the absorber plate (condensing board):

$$\rho_{pc}c_{p,pc}\frac{\partial T_{pc}}{\partial t}=k_{pc}\frac{\partial^2 T_{pc}}{\partial z^2}+\frac{4}{\pi\left(D_{pc,out}^2-D_{pc,in}^2\right)}\left(\pi D_{pc,in}K_{ref-pc}\left(T_{ref}-T_{pc}\right)+K_{pc-bc}l_{pc-bc}\left(T_{bc}-T_{pc}\right)\right) \quad (4)$$

$K_{ref-pc}$ and $K_{pc-bc}$ are the heat transfer coefficients between the refrigerant and the condensing pipe, condensing pipe and the condensing board; $l_{pc-bc}$ is the welding width of the condensing pipe.

The absorber board in the MCHP/TEG condenser collects heat from the condensing pipe and transfers it to the MCHP (evaporating section):

$$\rho_{bc}c_{p,bc}\frac{\partial T_{bc}}{\partial t}=k_{bc}\frac{\partial^2 T_{bc}}{\partial y^2}+k_{bc}\frac{\partial^2 T_{bc}}{\partial x^2}+\frac{1}{\delta_{bc}}\left(K_{MCHP-bc}\left(T_{MCHP,e}-T_{bc}\right)+\frac{K_{pc-bc}l_{pc-bc}\left(T_{pc}-T_{bc}\right)}{dx}\right) \quad (5)$$

$K_{MCHP-bc}$ is the heat transfer coefficient between the MCHP and the board; $T_{MCHP,e}$ and $T_{MCHP,c}$ are the temperatures in the evaporating section and condensing section of the MCHP.

The heat calculation of the MCHP[32]:

The evaporating part:

$$M_{MCHP,e}c_p\frac{\partial T_{MCHP,e}}{\partial t}=k_{MCHP}l_{MCHP}\left(T_{MCHP,c}-T_{MCHP,e}\right)+K_{MCHP-bc}A_{MCHP-bc}\left(T_{bc}-T_{MCHP,e}\right) \quad (6)$$

The condensing part:

$$M_{MCHP,c}c_p\frac{\partial T_{MCHP,c}}{\partial t}=k_{MCHP}l_{MCHP}\left(T_{MCHP,e}-T_{MCHP,c}\right)+\dot{Q}_{high} \quad (7)$$

The evaporating part of the MCHP collects heat from the board and conducts it to the condensing part. The condensing part gets the heat and releases it onto the hot surface of the TEG. $k_{MCHP}$ and $l_{MCHP}$ are the comprehensive thermal conductivity and length of the MCHP; $A_{MCHP-bc}$ is the contact area of the MCHP and the board. $\dot{Q}_{high}$ is the heat flow rate in the high-temperature segment of TEG comes from MCHP, part of which is transferred into electricity while the rest is conducted to the water through the low-temperature segment of TEG and water channel.

The TEG calculation[33, 34]:

$$\dot{Q}_{high} = S \cdot T_{high} \frac{S\left(T_{high} - T_{low}\right)}{2R} + \frac{T_{high} - T_{low}}{R_t} - \frac{I^2 R}{2} = \frac{k_j A_{TEG}\left(T_{MCHP,c} - T_{high}\right)}{\delta_j} \tag{8}$$

$$\dot{Q}_{low} = S \cdot T_{low} \frac{S\left(T_{high} - T_{low}\right)}{2R} + \frac{T_{high} - T_{low}}{R_t} + \frac{I^2 R}{2} \tag{9}$$

$$P_{TEG} = \dot{Q}_{high} - \dot{Q}_{low} = \frac{S^2\left(T_{high} - T_{low}\right)^2}{4R} \tag{10}$$

$S$, $R_t$, and $R$ are total Seebeck coefficient, thermal resistance, and electrical resistance, while $T_{low}$ and $T_{high}$ are the temperatures of two surfaces of TEG; $A_{TEG}$ is the surface area of TEG; $k_j$ and $\delta_j$ are the thermal conductivity and the thickness of the silica gel. Table.3 lists the commercial factors of the TEG model used in the test, whose type is TGM-287-1.4-1.5.

Table.3 The parameters of TGM-287-1.4-1.5 ($T_{high}$=200□, $T_{low}$=30□)

| Parameters | Values |
|---|---|
| Height | 4.2mm |
| Size | 55mm×55mm |
| Thermal resistance | 0.85K/W |
| Electrical resistance | 5.0Ω |
| Short circuit current | 1.65A |
| Open circuit voltage | 12.2V |

The water channel transfers the collected heat from the low-temperature segment of TEG to the inner flowing water:

$$\rho_{wc} c_{p,wc} \frac{\partial T_{wc}}{\partial t} = k_{wc} \frac{\partial^2 T_{wc}}{\partial z^2} + \frac{1}{A_{wc}}\left(CK_{wc-w}\left(T_w - T_{wc}\right) + \frac{\dot{Q}_{low}}{dz}\right) \tag{11}$$

$C$ and $A_{wc}$ are cross-sectional wet cycle and area of the water channel; $K_{wc-w}$ is the heat transfer coefficient between the water and the water channel.

In the channel, the water meets the following equation:

$$A_w \rho_w c_{p,w} \frac{\partial T_w}{\partial t} = k_w A_w \frac{\partial^2 T_w}{\partial z^2} + CK_{wc-w}\left(T_w - T_{wc}\right) - \dot{m}_w c_{p,w} \frac{\partial T_w}{\partial z} \tag{12}$$

$\dot{m}_w$ is the water mass flow rate; $A_w$ is the water flow cross-sectional area.

***The coil condenser part:***

The refrigerant that is not fully cooled in the MCHP/TEG condenser would release heat to the water in the tank. The coil exchanges heat with the inner refrigerant and the outer water:

$$\rho_{pc}c_{p,pc}\frac{\partial T_{pc}}{\partial t}=k_{pc}\frac{\partial^2 T_{pc}}{\partial z^2}+\frac{4}{\pi\left(D_{pc,out}^2-D_{pc,in}^2\right)}\left(\pi D_{pc,in}K_{ref-pc}\left(T_{ref}-T_{pc}\right)+\pi D_{pc,out}K_{w-pc}\left(T_w-T_{pc}\right)\right) \quad (13)$$

The water in the tank would dissipate heat to the ambient through the tank, while collecting heat from the refrigerant in the coil and the water in the water channel in the MCHP/TEG section:

$$M_w c_{p,w}\frac{\partial T_w}{\partial t}=A_{wt}K_{wt-a}\left(T_a-T_w\right)+\dot{m}_{ref}\left(h_{wt,il}-h_{wt,ol}\right)+\dot{m}_w c_{p,w}\left(T_{w,ol}-T_{w,il}\right) \quad (14)$$

$A_{wt}$ and $K_{wt-a}$ are the effective heat transfer area and the comprehensive heat transfer coefficient of the water tank; $\dot{m}_{ref}$ and $\dot{m}_w$ are the mass flow rates of the refrigerant and the water; $h_{wt,il}$ and $h_{wt,ol}$ are the specific enthalpies of the refrigerant at the inlet and outlet of the water tank; $T_{w,il}$ and $T_{w,ol}$ are the water temperatures at the inlet and outlet of the water channel.

The calculation of the capillary, compressor, and refrigerant could refer to the last paper[30].

### 3.3 Evaluation

The PV efficiency of the system is the ratio of the PV output to the total received irradiation on the evaporating surface:

$$\eta_{pv}=\frac{P_{pv}}{AG} \quad (15)$$

The total electrical efficiency of the system is the ratio of the sum of PV output and TEG output to the total received irradiation:

$$\eta_e=\frac{P_{pv}+P_{TEG}}{AG} \quad (16)$$

$A$ is the surface area of the PV evaporator plate; $G$ is the irradiance.

Heating capacity:

$$\dot{Q}=M_w c_{p,w}\left(T_w^{t+\Delta t}-T_w^t\right)/\Delta t \quad (17)$$

Net electrical consumption:

$$P_{net}=P_{com}-(P_{pv}+P_{TEG}) \quad (18)$$

Since the system could produce more than one form of energy, the hybrid coefficient of performance $COP_{PVT}$ and the traditional coefficient of performance $COP_{th}$ are both adopted to value the system [35-39]:

$$COP_{th}=\frac{\dot{Q}}{P_{com}} \quad (19)$$

$$COP_{PVT} = \frac{\dot{Q} + (P_{pv} + P_{TEG}) / 0.38}{P_{com}} \tag{20}$$

Where 0.38 is the generally adopted conversion efficiency for a standard thermal power plants[40].
The definition of the net energy efficiency ratio (NEER):

$$NEER = \frac{\dot{Q}}{P_{net}} \tag{21}$$

The solar exergy calculations for isotropic blackbody radiation reservoirs have been concluded in [41]. But for the photovoltaic surface here, which is not a blackbody, the calculation equation is corrected as Eq.(22) in [42].

$$\dot{E}x_{solar} = \left(1 - \frac{4T_{air}}{3T_{sun}} - \left(\frac{i_3(b_{\mu 0}, b_{g0}, \infty) + j_2(b_{\mu 0}, b_{g0}, \infty)}{6.4939}\right) \times \left(\frac{T_{air}}{T_{sun}}\right)^4\right) A_g G \tag{22}$$

$$T_{sun} = 6000K \tag{23}$$

Where the functions $i_3$ and $j_2$ are calculated as:

$$i_3(b_{\mu 0}, b_{g0}, \infty) = \int_{b_{g0}}^{\infty} \frac{b^3 db}{\exp\left(b - b_{\mu 0}\right) - 1} \tag{24}$$

$$j_2(b_{\mu 0}, b_{g0}, \infty) = \int_{b_{g0}}^{\infty} \left(\tilde{n}(b) \ln\left(\tilde{n}(b)\right) - \left(1 + \tilde{n}(b)\right) \ln\left(1 + \tilde{n}(b)\right)\right) b^2 db \tag{25}$$

$$\tilde{n}(b) = \left(\exp(b - b_{\mu 0}) - 1\right)^{-1} \tag{26}$$

$$b_{g0} = e_g / \left(kT_0\right) \tag{27}$$

$$b_{\mu 0} = \left(qV^0\right) / \left(kT_0\right) \tag{28}$$

In which, the $e_g$, $V_0$, and $T_0$ are the band-gap energy, the voltage across the cell, and the cell temperature, respectively.
The heat exergy per $\Delta t$ generated in the water tank is calculated as Eq.(29)[43]:

$$\dot{E}x_{th} = \left(1 - \frac{T_a}{T_w}\right) \dot{Q} \tag{29}$$

Where the $T_w$ is the instantaneous water temperature, $\dot{Q}$ is the obtained heat in $\Delta t$ when water temperature is $T_w$.

Electrical energy could be equivalently transformed to exergy.

$$\dot{E}x_{PV} = P_{pv} \tag{30}$$

$$\dot{E}x_{TEG} = P_{TEG} \tag{31}$$

According to the definition: total exergy output is divided by total exergy input [44]. Exergy efficiency is calculated as:

$$\vartheta_{PVT} = \frac{\dot{E}x_{PV} + \dot{E}x_{TEG} + \dot{E}x_{th}}{\dot{E}x_{solar} + \dot{E}x_{com}} \tag{32}$$

## 4. Validation

The experiment data is recorded on May 29th from 10:49 to 13:29 and May 30th from 9:58 to 12:15 in Hefei (latitude 31°N, longitude 117°E), China. The ambient conditions are presented in Fig.5.

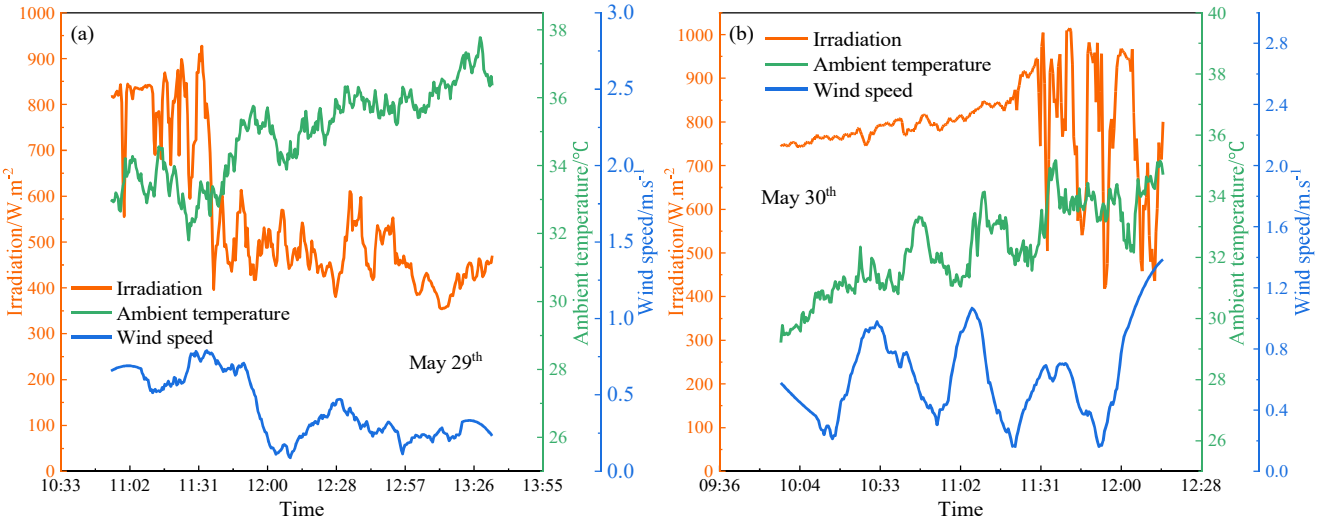


Fig.5 Ambient conditions during the test

The calculated electrical performance of the PV and the TEG, the water temperature change, and compressor power consumption are compared with the experiment data on May 29th and May 30th, which are presented in Fig.6 and Fig.7.

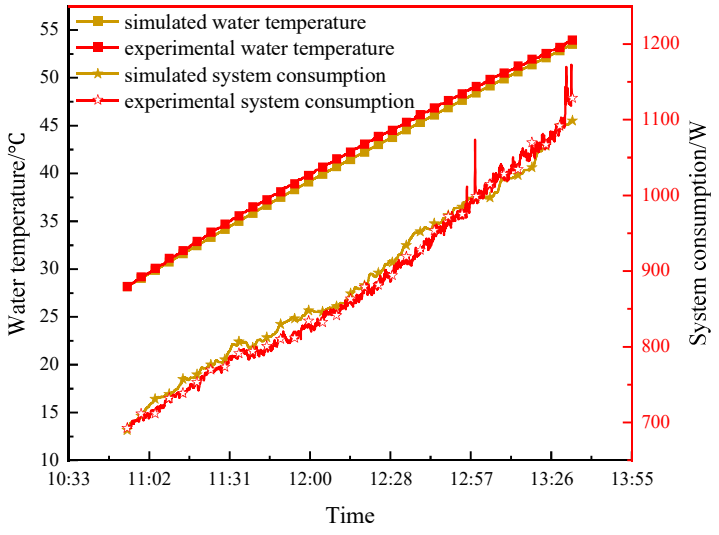


(a)

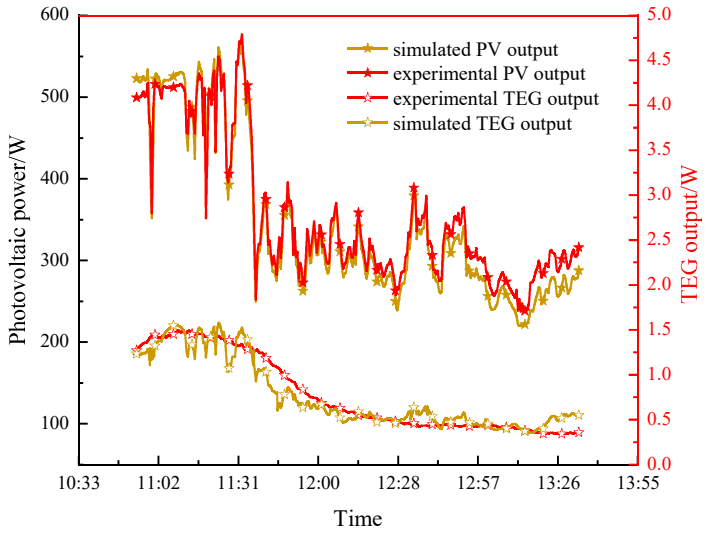


(b)

Fig.6 The model validation on May 29th

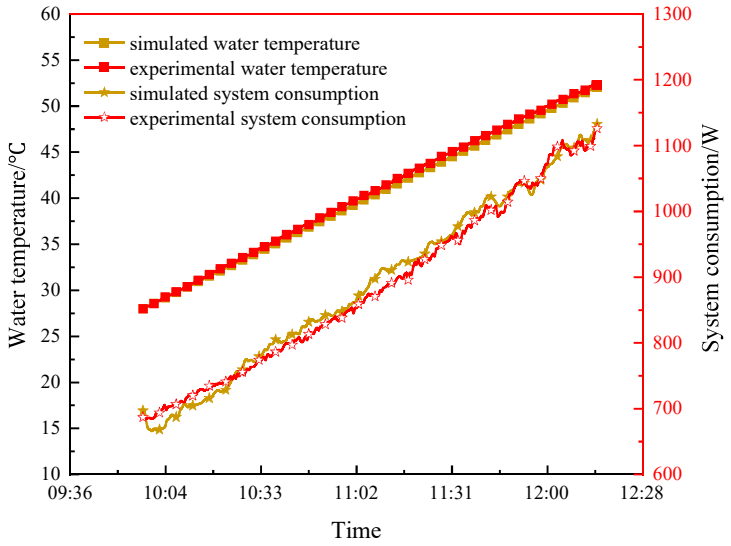


(a)

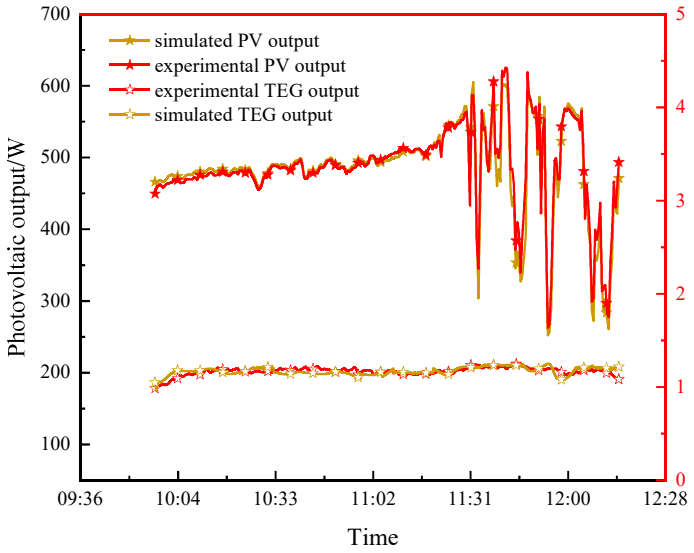


(b)

Fig.7 The model validation on May 30th

To demonstrate the precision, the root mean square deviations (RMSD) of the compared parameters shown above are calculated as follows:

$$RMSD = \sqrt{\frac{\sum_{i=1}^{n}\left(\frac{X_{\exp,i} - X_{sim,i}}{X_{\exp,i}}\right)^2}{n}} \tag{33}$$

$X_{sim,i}$ - simulated data; $X_{\exp,i}$ - experiment data. On May 30th, the RMSDs of the TEG power, PV power, compressor power, and water temperature are 3.59%, 3.45%, 1.79%, and 1.94%, which are 20.28%, 6.32%, 1.71%, and 1.45% on May 29th. Among them, only the calculated TEG power on May 29th is relatively high because of the unstable ambient conditions, while the other data shows good fitness.

Thus, the mathematical model could be used for performance prediction.

## 5. Results and discussion

To investigate the annual performance of the proposed PV-DC-SAHP system at different weather conditions, three cities with different latitudes are selected: Beijing (40°N, 116°E), Hefei (32°N, 117°E), and Hongkong (22°N, 114°E). Besides, Garze (32°N, 100°E) is also considered, which is located at almost the same latitude as Hefei but has better solar energy due to its high altitude.

From previous analysis, replacing the TEG model with better parameters could optimize the system's output. As a result, in this section, the TEG parameters are replaced by the ones obtained from Wu's paper[34], listed in Table.2.

Besides, from the previous study[45], it was found that refrigerant mass injection has a great impact on system performance. For annual analysis, the operating environment of the PV-DC-SAHP system varies greatly in different seasons. Thus, the total refrigerant mass in the cycle could be quite different under different conditions. For this reason, the refrigerant mass is always modified according to the refrigerant status at the evaporator outlet to realize the optimization of the annual performance.

### 5.1 The electricity performance

The solar irradiance is extremely important for the performance of the PV direct-expansion heat pump. So the heat pump system only operates when the irradiance is higher than 100W/$m^2$. The weather conditions of the four cities are shown in Fig.8 and Fig.9. The values in the figures are calculated based on the weather conditions during the operating period. Fig.8 shows that in Hefei, the irradiation is better in spring and autumn, and the highest daily mean total irradiation is 15.9MJ/$m^2$ in July, while the lowest one is in January at 8.5MJ/$m^2$. For Beijing, the irradiation reaches its peak in the spring, and 18.6MJ/$m^2$ daily mean total irradiation is obtained in May, while it reaches its lowest level of 11.7 MJ/$m^2$ in December. As for Hongkong, the peak period of the irradiation occurs from late summer to fall, and the highest value is 16.5MJ/$m^2$ in July, while the lowest value is 10.3 MJ/$m^2$ in March. Garze has the richest solar energy resources among the selected cities, and the daily mean total irradiation is always the highest at around 20MJ/$m^2$, which only slightly drops during summer. During the year, the value varies from 19.1MJ/$m^2$ to 22.3MJ/$m^2$. In the first half of the year, apart from the highest irradiation in Garze, Beijing owns the second highest daily irradiation, while that in Hongkong is almost the lowest. In the later half of the year, Garze still has the best solar irradiation, yet the solar irradiation in Hongkong is the second highest and the solar irradiation in Hefei is the lowest. The ambient temperatures in the four cities show a similar trend throughout the year: increase first and then decrease, and the temperature peaks in the summer. During the temperature peak time of the year (around summer), the temperatures at Hefei, Beijing, and Hongkong are similar at around 30□, while

that in Garze is apparently lower than the others because of the high altitude, stable at 15~20□. During the winter, the temperatures of Hefei, Garze, and Beijing are close, but Hongkong is much warmer than the others due to the lowest latitude and its location beside the sea. As a result, Hongkong has the highest annual temperature, while that of Garze is the lowest. The temperature in Hefei is similar to that in Beijing but a little warmer.

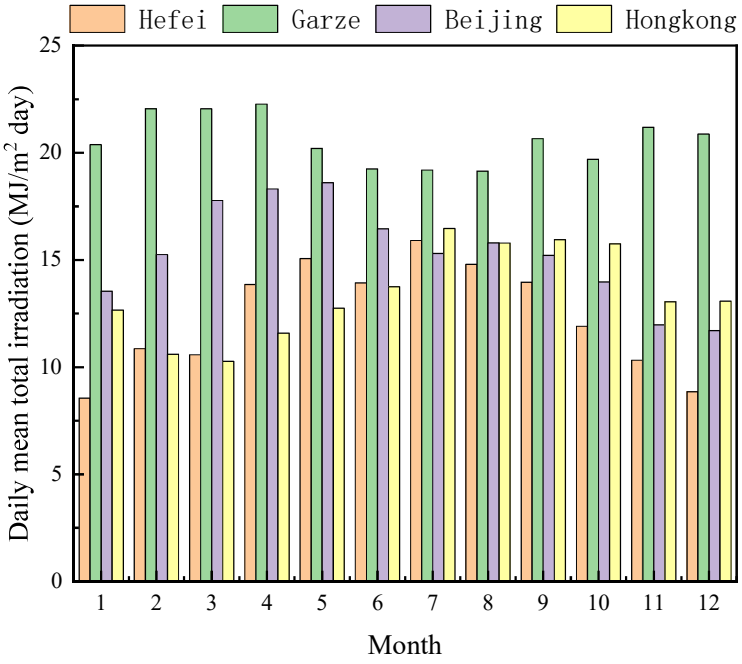


Fig.8 The daily mean total irradiation per month in the four cities

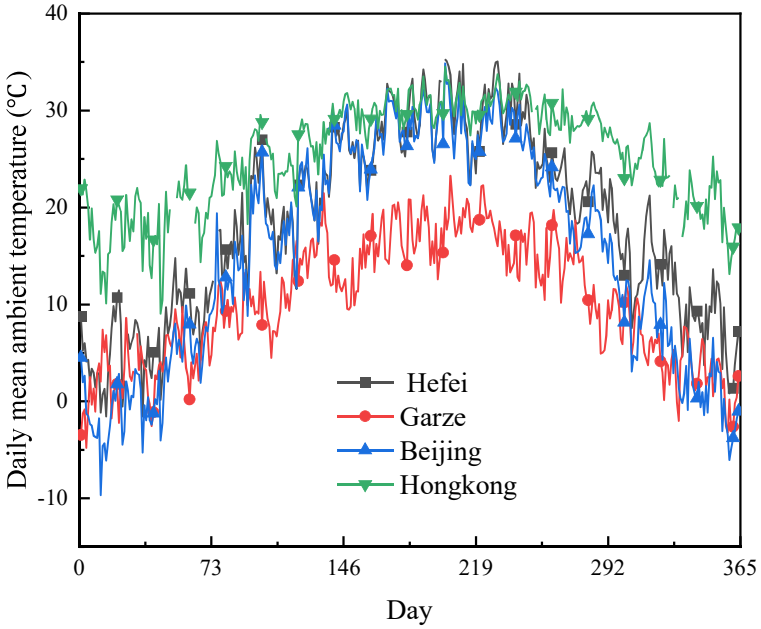


Fig.9 The daily mean ambient temperature during the year of the four cities

Fig.10 shows the PV, TEG, and total electrical output amounts in each month at different cities. In the figure, the PV electricity means the electricity purely generated by the PV cells; the TEG electricity

means the electricity generated by TEG in the system; and the total electricity is the sum of the PV and TEG generation. From the figures, the electricity generated by TEG rises initially, drops during the year, and peaks mainly in the middle of the year. The TEG output is highly impacted by two factors: irradiation and ambient temperature. The change of TEG's monthly power production in Garze is gentler than that in other regions because of the more stable irradiation and ambient temperature throughout the year. In Hongkong, the annual environmental temperature is warmer than that in Beijing and Hefei, so the TEG power generation in Hongkong during the winter is higher than that in Hefei and Beijing.

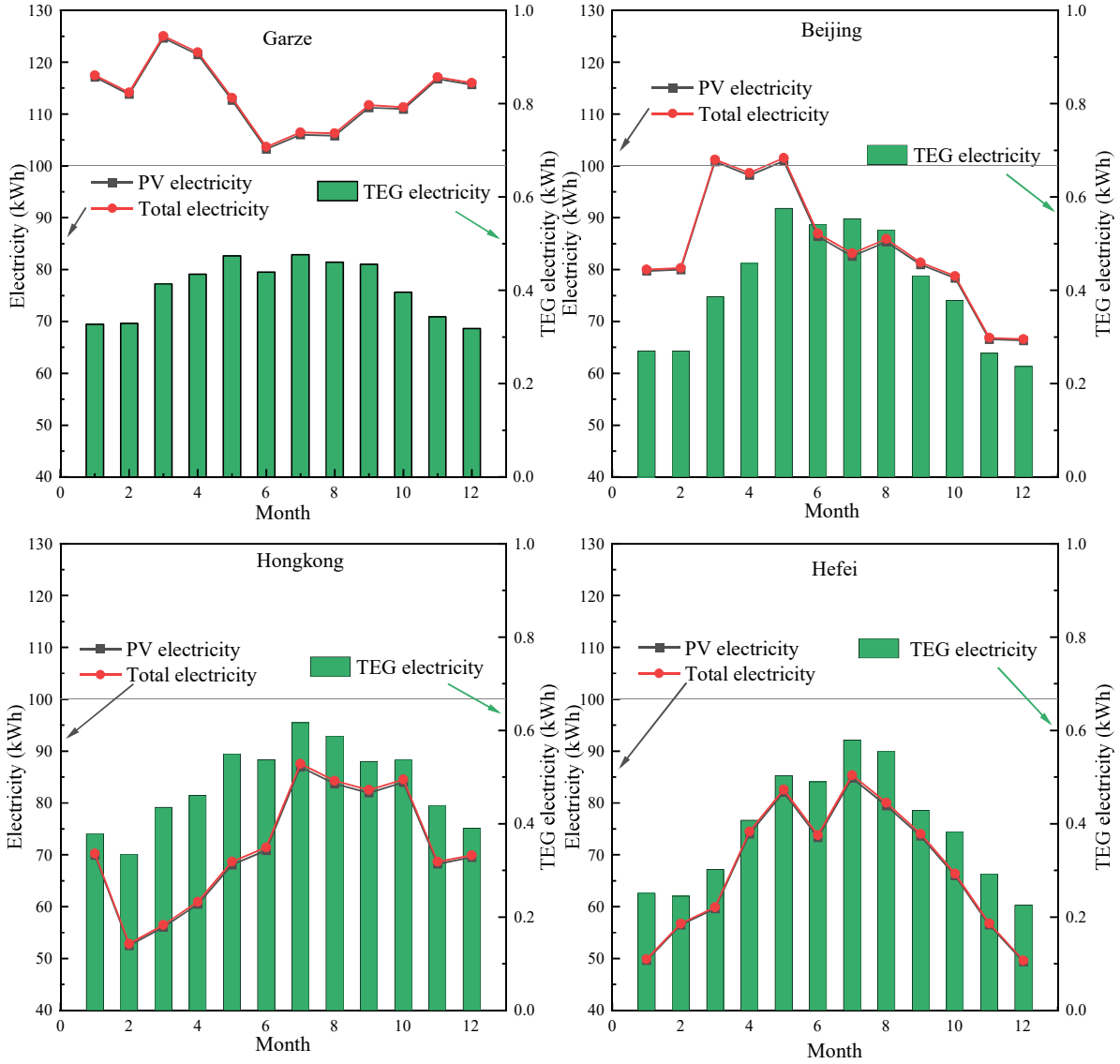


Fig.10 The electrical performance of the system at different cities

Furthermore, due to higher irradiation in Hong Kong from July to October, the TEG's power generation is higher during the four months. In Hefei, both the temperature and the irradiation reach higher values in the summer. Thus, summer is the peak period of TEG output. In the four cities, the highest TEG power output is 0.58kWh in July in Hefei, 0.48kWh in July in Garze, 0.62kWh in July in Hongkong, and 0.58kWh in May in Beijing, respectively. In the whole system, the electrical power output mainly

depends on the PV generation, but the additional TEG power generation makes the total electricity generation slightly higher than the pure PV power output. The primary factor that dominates PV power generation is irradiation. In Garze, the monthly electrical output is always high, all above 100kWh per month, and the peak power generation period lasts from January to April, with the highest value of 125kWh in March. Even the lowest power generation is still as high as 104kWh in June. In Beijing, the power generation is apparently higher from March to May, with a peak value of 102kWh in May, which is still lower than the lowest power generation in Garze. In both Hongkong and Hefei, the monthly power generation never exceeds 100kWh. The peak power generation period in Hong Kong is from July to October, with a peak of 88 kWh in July, while the best time in Hefei is during the middle of the year, with a peak of 85 kWh in July. For the four cities, except for Garze, winter is always the low-power generation period.

Fig.11 shows the PV and TEG power generation throughout the year in different cities. Garze owns the highest annual PV power generation of 1359kWh, followed by 1066kWh in Beijing, 852kWh in Hongkong, and 805kWh in Hefei. But for the TEG power generation, it presents different order. Benefiting from the higher annual ambient temperature, Hongkong owns the highest TEG power generation of 5.8kWh, while Hefei is the lowest at 4.7kWh, and the rest two are almost the same at 4.9kWh. In terms of the overall power generation, Garze with better irradiation still has the highest value, reaching 1364kWh per year.

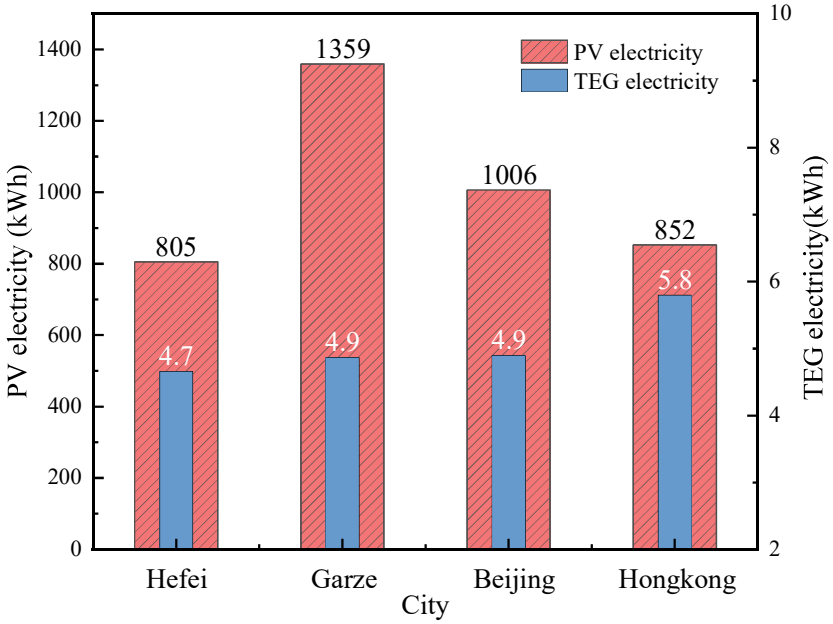


Fig.11 The PV and TEG power generation in a year

In Fig.12, the PV means the electricity purely generated by the PV cells, and the total means the sum of the PV and TEG generation. In Fig.12(a), for the four cities, a similar trend appears in the PV and total electrical efficiencies throughout the year: first decreasing and then increasing, which is mainly caused by the change of ambient temperature in different seasons. The air temperature in summer is the highest leading to the temperature increase in evaporator and PV. Due to the negative correlation

between photoelectric conversion efficiency and PV temperature, system electrical efficiency is lower in the summer compared with other periods. In the figure, the solid line is the PV electrical efficiency in different cities, and the dotted line is the total electrical efficiency. Due to additional thermoelectric generation, the total electrical conversion efficiencies in different cities are all higher. Benefiting from the lower ambient temperature in the middle of the year, the electrical efficiency in Garze is the highest during the period from April to October. At the beginning and end of the year, the ambient temperature in Garze is close to that in Hefei and Beijing, but its irradiation intensity is significantly higher. Thus, the electrical efficiency in Garze during these two periods is lower than that in Beijing and Hefei. In Beijing, due to its higher latitude, the annual temperature is slightly lower than that in Hefei. Therefore, its electrical efficiency is kind of higher than Hefei most of the time, except for the peak irradiation period in spring in Beijing. Resulting from the higher annual ambient temperature, the electrical efficiency in Hongkong is always the lowest among the selected cities. Fig.12(b) summarized the annual mean electrical efficiency in the four cities. The green area is the part contributed by TEG generation. From the figure, Hongkong has the lowest average electrical efficiency of 16.19% and the TEG generation has the highest contribution rate in this place, accounting for 0.6% of the total power generation. Garze has the highest annual electrical efficiency of 16.87% and the lowest TEG contribution to the total power generation. The annual electrical efficiency in Beijing is slightly better than that in Hefei.

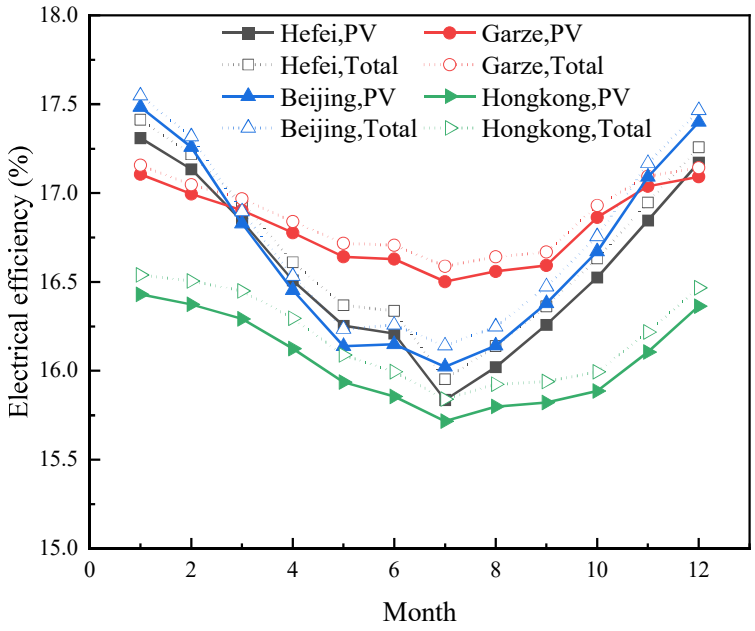


(a)

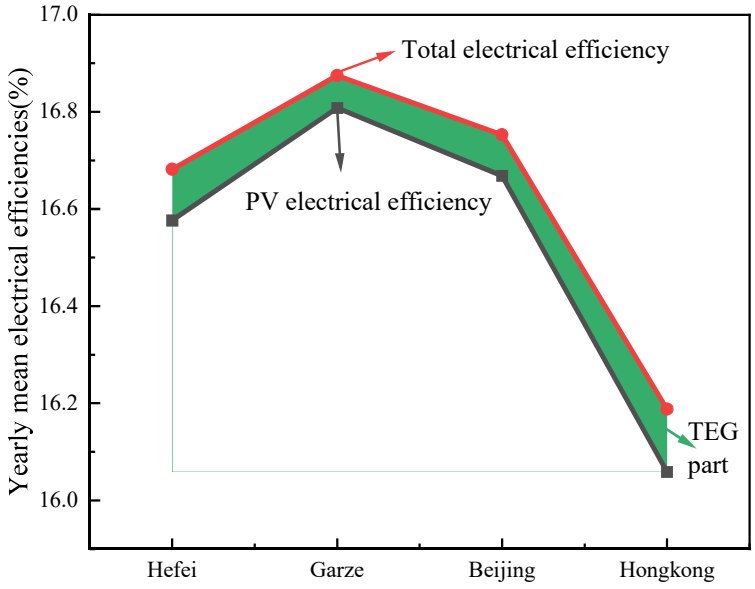


(b)

Fig.12 The monthly electrical efficiency of the system in different cities

## 5.2 Heating and energy consumption

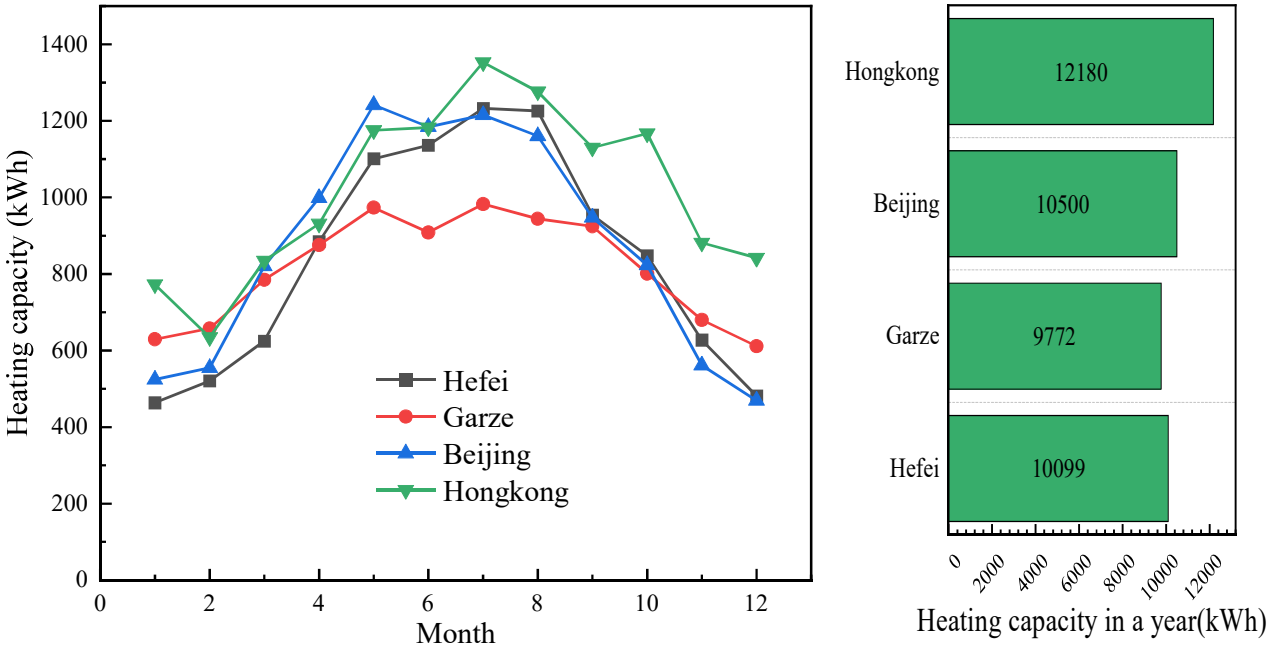


(a) (b)

Fig.13 The system heating capacity in different cities

Fig.13 shows the monthly and yearly system heating capacity in the four cities. Influenced by the change of ambient temperature throughout the year, the heating capacity in different cities all peaks at the middle of the year. The heating capacity is simultaneously influenced by temperature and irradiation. For Garze and Hongkong, the annual ambient temperature varies largely compared with the others, so the temperature impact dominates. Owing to the higher annual ambient temperature, the

system in Hongkong generates more heat at most times of the year. For the similar reason, Garze produces the lowest level of heat. From Fig.9, the ambient temperatures in Hefei and Beijing are the closest, and Hefei is a bit higher. But in Fig.13(a), before July, the heating capacity in Beijing is higher because of better irradiation in the former half of the year compared to that in Hefei. In the later half of the year, the irradiation gap between them gets smaller, and the ambient temperature impact is more primary, resulting in better heating capacity in Hefei. Because of the superimposed effects of irradiation, different cities get their peak values in different months. The heating capacity peaks at 1136kWh in July in Hefei, 982kWh in July in Garze, 1242kWh in May in Beijing, 1353kWh in July in Hongkong. On a year-round basis, as shown in Fig.13(b), Hongkong could produce the most heat with 12180kWh, followed by Beijing with a value of 10500kWh, and then 10099kWh in Hefei, while Garze is the lowest at 9772kWh.

Fig.14 illustrates the power consumption in different cities. Because of the higher air temperature in summer, the heating amount and evaporating temperature are higher, and the compressor power is also rising to the top during the middle of the year. Since the hybrid system is continuously generating electricity, which could make up for the consumed power to some extent, the net electricity depletion is largely eased. Among the four cities, the power depletion in Garze is the lowest, and benefiting from the good irradiation condition, the electrical generation is the highest. Consequently, the net electricity requirement is the lowest. Even during the peak period, the highest required net electricity is just 142kWh in July in Garze. While in the other areas, the compressor power consumption is higher and the electricity generation is lower, leading to a much bigger amount of net electricity expenditure. In Beijing, the net amount could be as high as 197kWh in July, while that is 201kWh in August in Hefei and 209kWh in July in Hongkong. On a year-round basis, the total power consumptions of the systems placed in ascending order are Hefei, Garze, Beijing, and Hongkong, with values of 2536kWh, 2623kWh, 2680kWh, and 2826kWh, respectively. However, the net power consumptions present a different order owing to different electricity generations, which are Garze, Beijing, Hefei, and Hongkong, with amounts of 1258kWh, 1668kWh, 1726kWh, and 1968kWh, respectively.

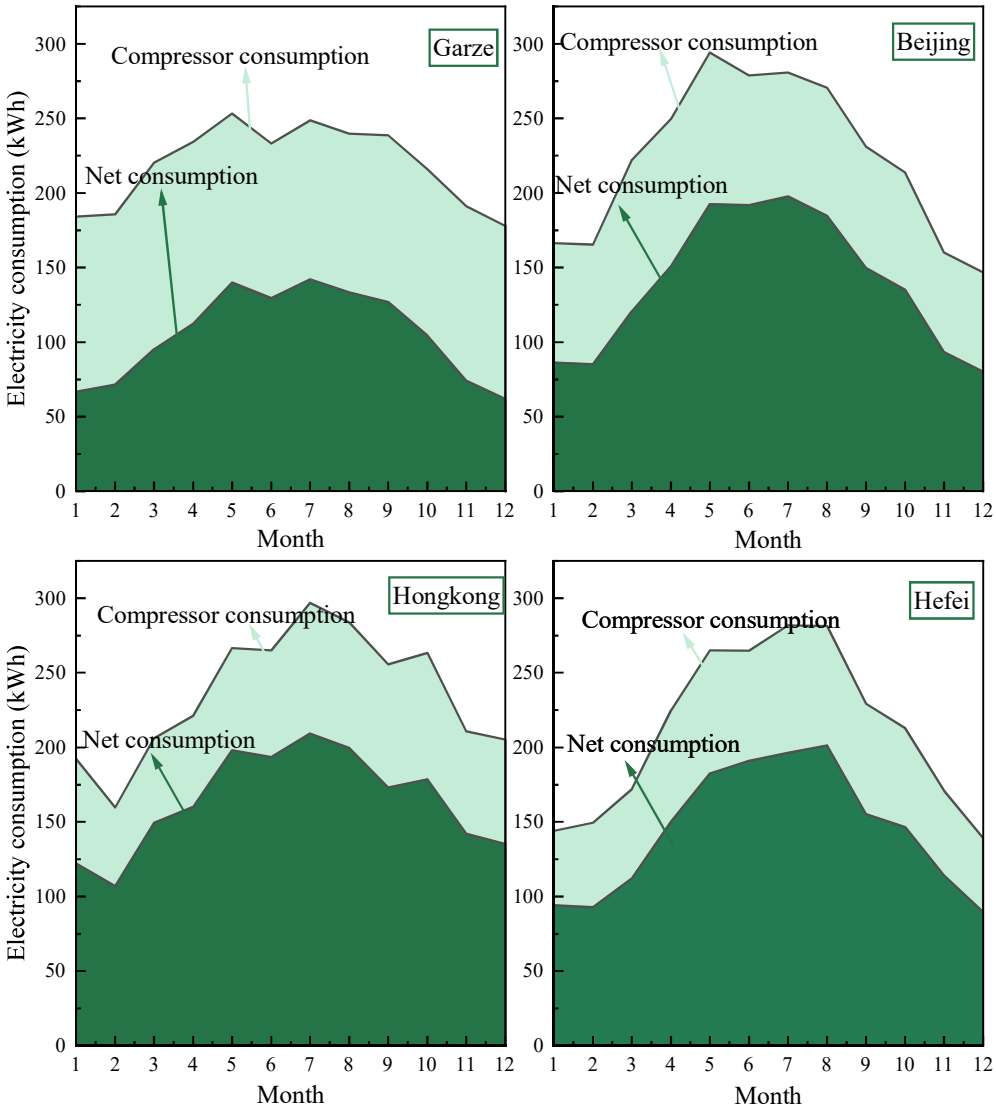
Garze
Beijing
Hongkong
Hefei
Compressor consumption
Net consumption
Electricity consumption (kWh)
Month

(a)

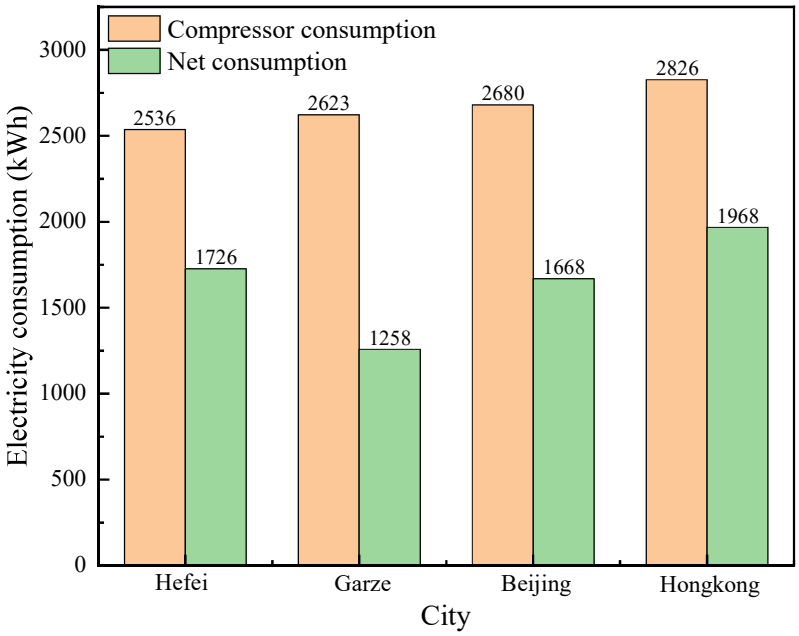
Compressor consumption
Net consumption
2536
1726
2623
1258
2680
1668
2826
1968
Electricity consumption (kWh)
Hefei
Garze
Beijing
Hongkong
City

(b)

Fig.14 The electrical consumption of the system in different cities

### 5.3 The coefficient of performance

For the heating $COP_{th}$ in Fig.15(a), in the middle of the year, with the higher temperature in the summer, the heating $COP_{th}$ in different cities reaches the highest value. Similar to the heating capacity, the $COP_{th}$ in Hongkong is the highest, which remains higher than 4, while that in Garze is the lowest, waving below 4. The difference of $COP_{th}$ in Hefei and Beijing is small. The highest values of $COP_{th}$ are all realized in July in different cities: 4.56 in Hongkong, 4.37 in Hefei, 4.33 in Beijing, and 3.95 in Garze. Taking electricity generation into account, as shown in Fig.15(b), the $COP_{PVT}$ is much higher than $COP_{th}$ in Garze, and it shows little seasonal change throughout the year, which is literally different with the other lines. Benefiting from the better irradiation condition, the $COP_{PVT}$ in Beijing is always higher than that in Hefei, much different from the $COP_{th}$ in Fig.15(a). In Fig.15(a), $COP_{th}$ in Hefei is higher than that in Beijing after June. During the summer and autumn, the irradiation in Garze declines but rises in Hongkong. The benefits of higher ambient temperature in Hongkong exceeds the boost of better irradiation in Garze during the period. As a result, the monthly mean $COP_{PVT}$ in Hongkong is better in the summer and autumn.

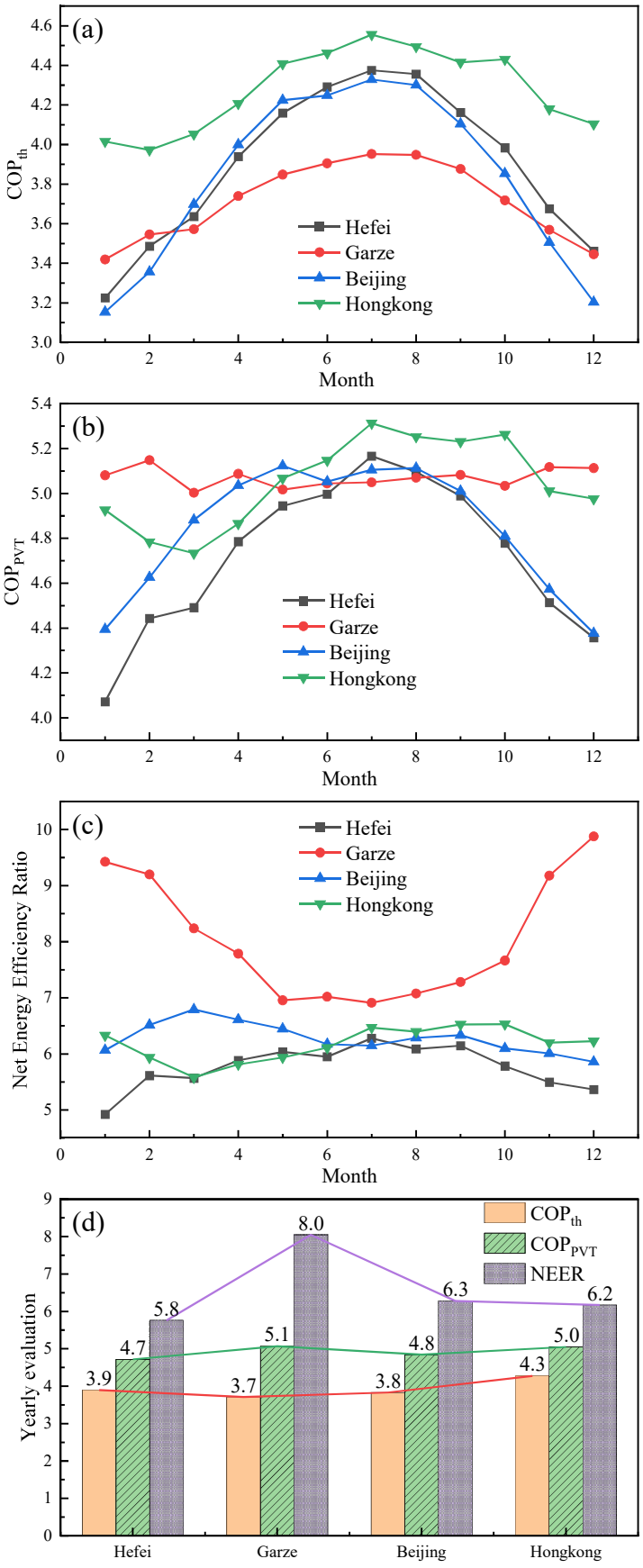


Fig.15 The COP of the system in different cities

In Fig.15(c), the heating capacity per unit of net electricity consumption is illustrated, and obviously,

the NEER is much higher in Garze compared with that in other cities, especially in the winter. The NEER could be as high as 9.9 in December in Garze. Although the irradiation is weaker and the system consumption is higher in the summer, the NEER can still remain above 7, whereas the monthly average NEER in the other three cities is always less than 7. The irradiation condition in the first half of the year is better in Beijing. Thus, the monthly NEER of Beijing is better than that in Hefei and Hongkong. In the second half of the year, the irradiation level in Hongkong is higher, so its NEER is better than that in Beijing and Hefei. Due to the poorest irradiation in Hefei, its NEER ranks at the bottom. For the year values in Fig.15(d), the annual $COP_{th}$ is better in Hongkong at 4.3, followed by that in Hefei, Beijing, and Garze. But for the annual $COP_{PVT}$, the best value is obtained in Garze, valued at 5.1, followed by Hongkong, Beijing, and Hefei. Meanwhile, the best yearly NEER is also obtained in Garze at 8.0, and the lowest value is in Hefei at 5.8.

Thus, in areas with a higher ambient temperature, the heating capacity and the $COP_{th}$ are higher, but at the same time, the power consumption also increases. In areas with better irradiation condition, the electricity production is better. Although the higher irradiation condition may not cover the attenuation of lower temperature on the heating performance, the $COP_{PVT}$ and the heating capacity per unit of net consumed power are greatly improved.

### 5.4 The exergy analysis

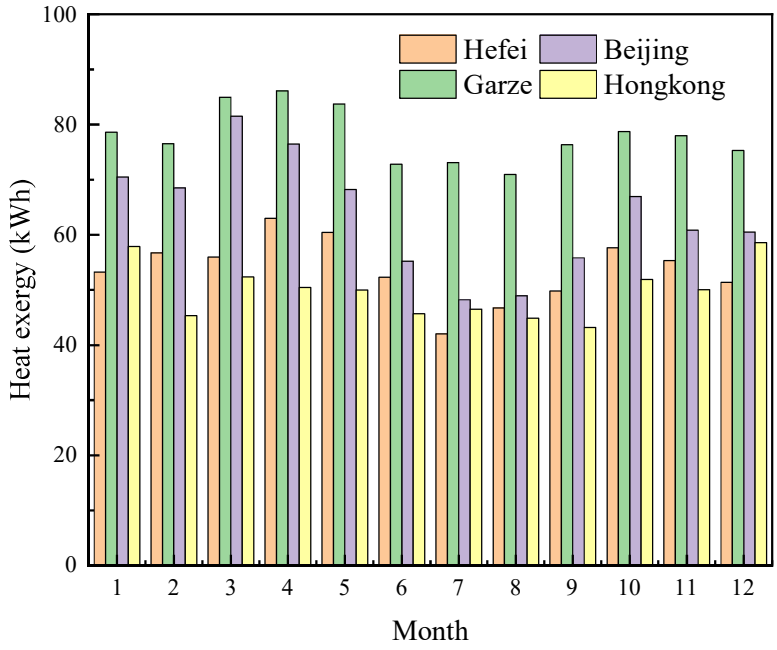


(a)

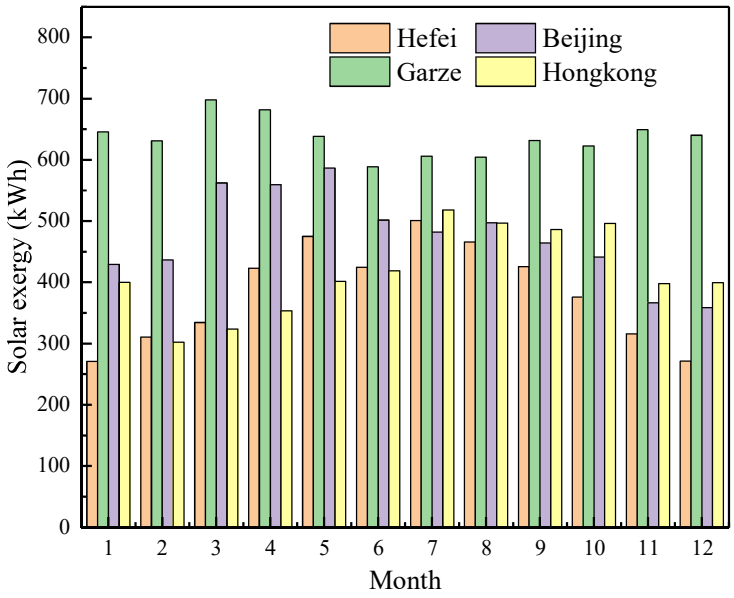


(b)

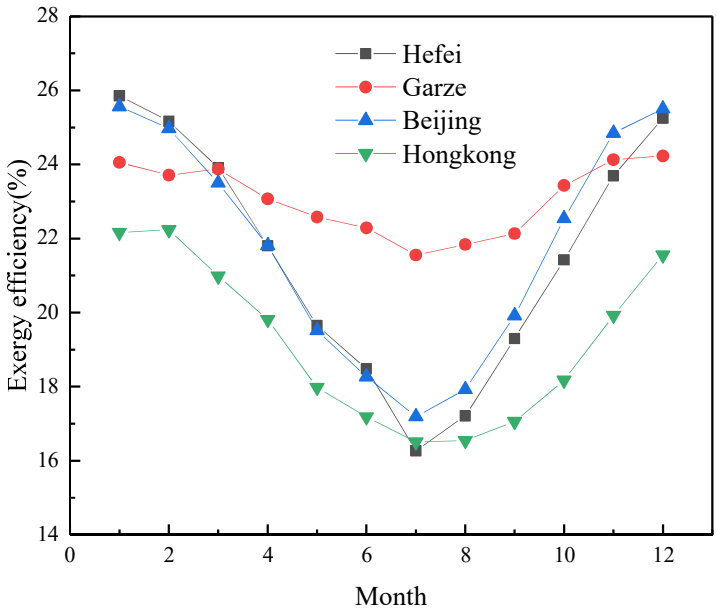


(c)

Fig.16 The exergy performance analysis ((a) the monthly heat exergy output; (b) the monthly solar exergy input; (c) the monthly exergy efficiency)

For the exergy analysis in Fig.16, when the water temperature is fixed, the lower the ambient temperature, the higher the temperature difference between the ambient and the water tank, meaning that the quality of the produced heat energy is better, and more mechanical work could be converted from heat according to Eq.(29). Thus, the heat exergy is influenced by the heating amount as well as the ambient temperature when the water temperature is assumed to be constant. Therefore, although the heating capacity in Hongkong is higher, the transferred heat exergy is the lowest because of the highest ambient temperature. The heat exergy in Garze is the highest, followed by Beijing and Hefei. It can also be observed that the peak period of heat exergy generation is always in the spring. The mean

monthly exergy generation throughout the year in the four cities are 77.9kWh, 63.5kWh, 53.7kWh, and 49.7kWh in turn.

Better irradiation leads to higher solar exergy input. Thus, the input solar exergy has a similar trend to the irradiation condition throughout the year. The solar exergy input in Garze maintains the highest level among the selected cities all year round, with a mean monthly value of 636.5kWh. In the first half of the year, the solar exergy input in Beijing is higher, while in the second half of the year, it is higher in Hongkong, and the mean monthly values are 473.9kWh and 416.2kWh, respectively. The electrical exergy consumed and generated by the system is numerically equivalent to the electricity presented in Fig.14 and Fig.10.

The monthly exergy efficiency is shown in Fig.16(c). In the summer, the monthly exergy efficiency is lower because the ambient temperature is higher, which means the mechanical energy conversion factor is lower. The lowest exergy efficiencies of the four cities are all obtained in July, with values of 16.27% in Hefei, 16.50% in Hongkong, 17.19% in Beijing, and 21.55% in Garze. In the spring and winter, the exergy efficiency is high. The top exergy efficiencies in the four cities are all obtained in the winter: 25.85% in January in Hefei, 24.23% in December in Garze, 22.23% in February in Hongkong, and 25.56% in January in Beijing. Among the four cities, in most months, the exergy efficiency in Garze is the highest and the monthly variation is the gentlest. Its mean annual exergy efficiency can reach 23.08%. On the contrary, the monthly exergy efficiency in Hongkong is always the lowest, and the annual exergy efficiency is only 19.14%. The exergy efficiencies in Hefei and Beijing are quite close to each other, and the seasonal variation is large. Their annual mean exergy efficiencies are 21.50% and 21.80%, respectively.

## 6. Economy and emissions

In this part, the comparison between the traditional gas boiler and the PV-DC-SAHP system on operating costs and carbon emissions is carried out. On a year-round basis, the volume of natural gas required by the gas boiler to produce the same amount of heat as the heat pump system in different cities is calculated. The corresponding costs and emissions are also calculated. Table.4 shows the prices and carbon emission factors of the electricity and nature gas. According to the GlobalPetrolPrices database, the electricity price for households in China is 0.546 RMB/kWh, and the natural gas price for residents updated in September 2022 in CEIC database is 2.66 RMB/$m^3$. The carbon emission factor (CF) of electricity in China is 0.55kg $CO_2$/kWh according to the data published on Statista site, and the CF of the natural gas is 1.95kg $CO_2/m^3$ according to EIA 2019, and it could release 37.62MJ heat per $m^3$. The total efficiency of the gas boiler (the percentage of the chemical energy which is converted into the thermal energy of water) is determined by two efficiencies: the gas combustion efficiency and the water absorption efficiency, and the total efficiency varies from 80% to almost 100% in commercial applications. Here it is adopted as 90%. Besides, to assess the energy-saving potential

of the proposed system, the consumed net electricity of the proposed system is converted into the required natural gas energy through the natural gas plant conversion efficiency, which is 0.45 obtained from EIA 2019.

Table.4 Parameters of the electricity and natural gas

| | Price (RMB) | CF (kg $CO_2$) | Combustion heat (MJ) |
|---|---|---|---|
| Natural gas ($m^3$) | 2.660 | 1.95 | 37.62 |
| Electricity (kWh) | 0.546 | 0.55 | |

The operating cost is calculated as the heating bill, which is net power consumption (or required gas volume)◊electricity price (or gas price). The carbon emission is net power consumption (or required gas volume)◊CF.

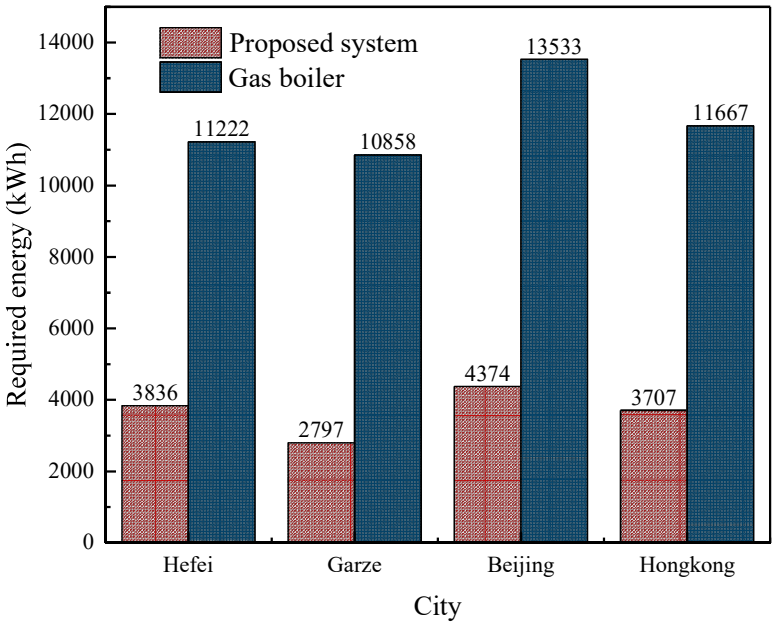


Fig.17 The energy consumption comparison

Fig.17 shows the required energy of the proposed heat pump system and the traditional gas boiler to produce the same amount of hot water in a year in different cities. For the traditional gas boiler, the required energy is obtained by: produced heat/gas boiler efficiency. For the proposed heat pump system, the required energy is obtained by: consumed net electricity for heat production/natural gas plant conversion efficiency. From Fig.17, it can be observed that the proposed system always requires less energy to produce the same amount of heat. In Hefei, the proposed system only needs 3836kWh natural gas energy, compared with 11222kWh for a traditional gas boiler to generate the same heating. That means the proposed system realizes 66% energy saving in Hefei, which is 74% in Garze and 68% in the other two cities. So this system could save 2/3~3/4 of the energy compared with the traditional gas boiler.

Fig.18 shows the operating cost of the proposed system and the gas boiler to produce the annual heating amount in different cities shown in Fig.13(b). To produce the same amount of heat with the heat pump

system, 1074m$^3$, 1039 m$^3$, 1116 m$^3$, and 1295 m$^3$ natural gas are required in Hefei, Garze, Beijing, and Hongkong, respectively. And the heating bills of the gas boiler are calculated as 2856RMB, 2764RMB, 2970RMB, and 3445RMB in the four cities, while the cost of the heat pump system is only 943RMB, 687RMB, 911RMB, and 1075RMB in a year, which are much lower. In Garze, the operating cost of PV-DC-SAHP is only one quarter of that of the traditional gas boiler, while the proportion is around one third in the other three cities. Fig.19 compares the carbon emissions of the two devices. In Hefei, Beijing, and Hongkong, the produced $CO_2$ could be reduced from 2090kg, 2520kg, and 2172kg to 949kg, 1038kg, and 918kg, which means more than half $CO_2$ emissions is cut off by replacing the gas boiler to the heat pump system. Moreover, in places with good irradiation, like Garze, the $CO_2$ emissions could be cut by about two-thirds, which could be of great help in reducing the greenhouse gas emissions.

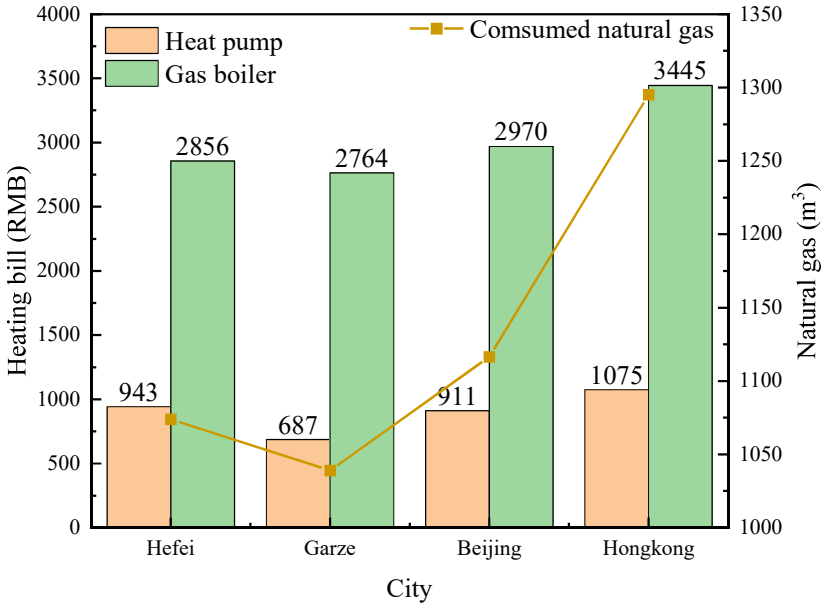


Fig.18 The heating bill comparison

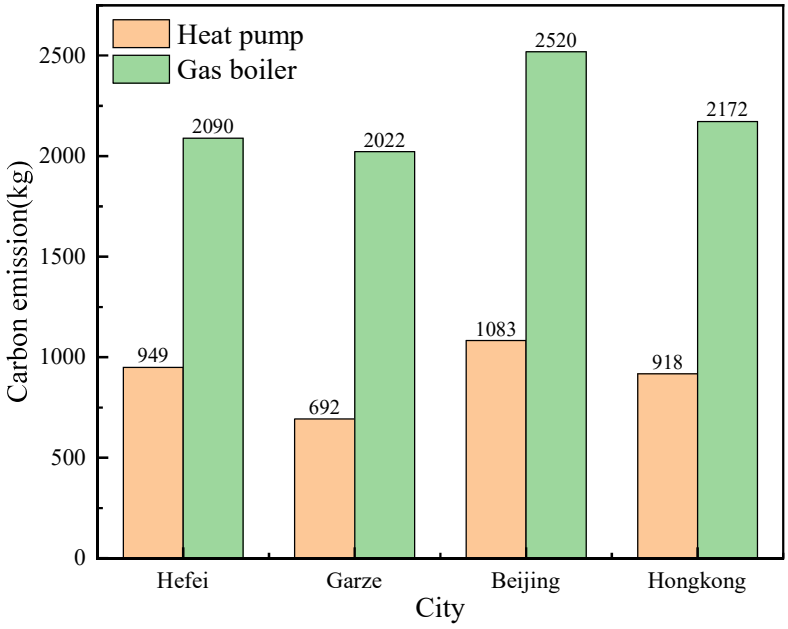

Fig.19 The emissions comparison

## 7. Conclusion

To avoid obstacles to PV heat dissipation while applying thermoelectric components, a photovoltaic direct expansion dual-condensing heat pump system combined with TEG assisted by micro-channel heat pipe is proposed. Based on the experiments & validated modelling, the annual performance of the system in Hefei, Garze, Beijing, and Hongkong is investigated. Besides, the annual heating cost and carbon emissions of this system and the traditional gas boiler are calculated and compared. Results are concluded:

(1) Better irradiation and lower ambient temperatures lead to better electrical performance. In Garze, the highest monthly electricity generation could be 125kWh, and the annual power generation is 1364kWh, which is much higher than 85kWh and 810kWh in Hefei. The highest annual electrical efficiency is 16.87% in Garze, while the lowest is in Hongkong at 16.19%;

(2) Higher ambient temperatures and irradiation are good for the TEG generation. When the ambient temperature is the highest in the middle of the year, the TEG generation will increase, and the highest value is always obtained in the month with better irradiation around the mid-year. With the highest annual ambient temperature, Hongkong could realize 5.7kWh TEG electricity generation in a year;

(3) Higher ambient temperatures result in increased heating capacity, while increased irradiation results in increased $COP_{PVT}$ and NEER. The annual heating capacity in Hongkong is the highest at 12180kWh, and the yearly $COP_{th}$ could be 4.3, but the compressor consumption is also the highest at 2826kWh. Benefitting from the great irradiation condition, the net electricity consumption is the lowest in Garze at 1258kWh, and the $COP_{PVT}$ as well as the NEER are much higher at 5.1 and 8.0;

(4) A Lower ambient temperature is good for the exergy efficiency. Over the whole year, lower exergy efficiency tends to occur when the ambient temperature is high in the middle of the year. The mean annual temperature in Garze is the lowest, and the yearly average exergy efficiency of 23.08% is realized;

(5) Compared with traditional gas boiler, the heat pump system could save 2/3~3/4 of the energy, reduce 2/3~3/4 of the heating cost, and lower 1/2~2/3 of the carbon emissions.

## Acknowledgement

This work is supported by the National Natural Science Foundation of China (No.52238004) and Anhui Provincial Major Science and Technology Project (202203a07020021).

# References


[1] H. Ritchie, M. Roser, CO2 and Greenhouse Gas Emissions., https://ourworldindata.org/co2-and-other-greenhouse-gas-emissions 2022.

[2] Y. Wang, C.-h. Guo, C. Du, X.-j. Chen, L.-q. Jia, X.-n. Guo, R.-s. Chen, M.-s. Zhang, Z.-y. Chen, H.-d. Wang, Carbon peak and carbon neutrality in China: Goals, implementation path, and prospects, China Geology 4(0) (2021) 1-27.

[3] U. DECC, The Future of Heating: A strategic framework for low carbon heat in the UK, Department of Energy and Climate Change London (2012).

[4] F. Zhang, J. Cai, J. Ji, K. Han, W. Ke, Experimental investigation on the heating and cooling performance of a solar air composite heat source heat pump, Renewable Energy 161 (2020) 221-229.

[5] China Building Energy Consumption and Carbon Emission Research Report ( 2021 ) , 2021. http://www.199it.com/archives/1369165.html.

[6] A. Shahsavari, M. Akbari, Potential of solar energy in developing countries for reducing energy-related emissions, Renewable and Sustainable Energy Reviews 90 (2018) 275-291.

[7] Q. Zhu, X. Chen, M. Song, X. Li, Z. Shen, Impacts of renewable electricity standard and Renewable Energy Certificates on renewable energy investments and carbon emissions, J Environ Manage 306 (2022) 114495.

[8] Z. Song, J. Ji, J. Cai, B. Zhao, Z. Li, Investigation on a direct-expansion solar-assisted heat pump with a novel hybrid compound parabolic concentrator/photovoltaic/fin evaporator, Applied Energy 299 (2021) 117279.

[9] C. Wang, Y. Gao, Z. Dai, D. Wu, Z. Huang, X. Zhang, L. Jiang, Experimental investigation and performance evaluation on a direct expansion solar-air source heat pump system, International Journal of Refrigeration (2022).

[10] C. Treichel, C.A. Cruickshank, Energy analysis of heat pump water heaters coupled with air-based solar thermal collectors in Canada and the United States, Energy 221 (2021).

[11] Y. Jiang, H. Zhang, Y. Wang, Y. Wang, M. Liu, S. You, Z. Wu, M. Fan, S. Wei, Research on the operation strategies of the solar assisted heat pump with triangular solar air collector, Energy 246 (2022).

[12] Y. Jiang, H. Zhang, Y. Wang, S. You, Z. Wu, M. Fan, L. Wang, S. Wei, A comparative study on the performance of a novel triangular solar air collector with tilted transparent cover plate, Solar Energy 227 (2021) 224-235.

[13] Y. Fan, X. Zhao, Z. Han, J. Li, A. Badiei, Y.G. Akhlaghi, Z. Liu, Scientific and technological progress and future perspectives of the solar assisted heat pump (SAHP) system, Energy 229 (2021) 120719.

[14] M. Lee, D. Lee, M.H. Park, Y.T. Kang, Y. Kim, Performance improvement of solar-assisted ground-source heat pumps with parallelly connected heat sources in heating-dominated areas, Energy 240 (2022).

[15] M. Lee, J. Kim, H.H. Shin, W. Cho, Y. Kim, CO2 emissions and energy performance analysis of ground-source and solar-assisted ground-source heat pumps using low-GWP refrigerants, Energy 261 (2022).

[16] J. Ji, K. Liu, T.-t. Chow, G. Pei, W. He, H. He, Performance analysis of a photovoltaic heat pump, Applied Energy 85(8) (2008) 680-693.

[17] N. Gunasekar, M. Mohanraj, V. Velmurugan, Artificial neural network modeling of a photovoltaic-thermal evaporator of solar assisted heat pumps, Energy 93 (2015) 908-922.

[18] S. abbas, Y. Yuan, A. Hassan, J. Zhou, C. Zeng, M. Yu, B. Emmanuel, Experimental and numerical investigation on a solar direct-expansion heat pump system employing PV/T & solar thermal collector as evaporator, Energy 254 (2022).

[19] Z. Song, J. Ji, J. Cai, Z. Li, B. Yu, The performance comparison of the direct-expansion solar assisted heat pumps with three different PV evaporators, Energy Conversion and Management 213 (2020) 112781.

652 [20] J. Yao, E. Chen, Y. Dai, M. Huang, Theoretical analysis on efficiency factor of direct expansion PVT module
653 for heat pump application, Solar Energy 206 (2020) 677-694.
654 [21] J. Yao, P. Dou, S. Zheng, Y. Zhao, Y. Dai, J. Zhu, V. Novakovic, Co-generation ability investigation of the
655 novel structured PVT heat pump system and its effect on the “Carbon neutral” strategy of Shanghai, Energy
656 239 (2022).
657 [22] L. Keliang, J. Jie, C. Tin-tai, P. Gang, H. Hanfeng, J. Aiguo, Y. Jichun, Performance study of a photovoltaic
658 solar assisted heat pump with variable-frequency compressor – A case study in Tibet, Renewable Energy 34(12)
659 (2009) 2680-2687.
660 [23] T.T. Chow, G. Pei, K.F. Fong, Z. Lin, A.L.S. Chan, M. He, Modeling and application of direct-expansion
661 solar-assisted heat pump for water heating in subtropical Hong Kong, Applied Energy 87(2) (2010) 643-649.
662 [24] H. Zhu, R. He, J. Mao, Q. Zhu, C. Li, J. Sun, W. Ren, Y. Wang, Z. Liu, Z. Tang, A. Sotnikov, Z. Wang, D.
663 Broido, D.J. Singh, G. Chen, K. Nielsch, Z. Ren, Discovery of ZrCoBi based half Heuslers with high
664 thermoelectric conversion efficiency, Nat Commun 9(1) (2018) 2497.
665 [25] H. Zhang, H. Yue, J. Huang, K. Liang, H. Chen, Experimental Studies on a Low Concentrating
666 Photovoltaic/Thermal (LCPV/T) Collector with a Thermoelectric Generator (TEG) Module, Renewable Energy
667 (2021).
668 [26] S. Shittu, G. Li, X. Zhao, J. Zhou, X. Ma, Y.G. Akhlaghi, Experimental study and exergy analysis of
669 photovoltaic-thermoelectric with flat plate micro-channel heat pipe, Energy Conversion and Management 207
670 (2020) 112515.
671 [27] X. Wen, J. Ji, Z. Song, Z. Li, H. Xie, J. Wang, Comparison analysis of two different concentrated
672 photovoltaic/thermal-TEG hybrid systems, Energy Conversion and Management 234 (2021) 113940.
673 [28] Z. Song, J. Ji, Z. Li, Performance of a heat pump system in combination with thermoelectric generators,

674 Energy 239 (2022) 121900.
675 [29] Z. Song, J. Ji, J. Cai, Z. Li, K. Han, Performance analyses on a novel heat pump with a hybrid condenser
676 combined with flat plate micro-channel heat pipe plus TEG and FPV evaporator, Energy Conversion and
677 Management (2020) 113606.
678 [30] Z. Song, J. Ji, Y. Zhang, J. Cai, Z. Li, Experimental and numerical investigation on a photovoltaic heat pump
679 with two condensers: A micro-channel heat pipe/thermoelectric generator condenser and a submerged coil
680 condenser, Energy (2021) 122525.
681 [31] X.F. Zheng, C.X. Liu, Y.Y. Yan, Q. Wang, A review of thermoelectrics research – Recent developments
682 and potentials for sustainable and renewable energy applications, Renewable and Sustainable Energy Reviews
683 32 (2014) 486-503.
684 [32] G. Li, G. Zhang, W. He, J. Ji, S. Lv, X. Chen, H. Chen, Performance analysis on a solar concentrating
685 thermoelectric generator using the micro-channel heat pipe array, Energy Conversion and Management 112
686 (2016) 191-198.
687 [33] G. Li, K. Zhou, Z. Song, X. Zhao, J. Ji, Inconsistent phenomenon of thermoelectric load resistance for
688 photovoltaic–thermoelectric module, Energy Conversion and Management 161 (2018) 155-161.
689 [34] Y.-Y. Wu, S.-Y. Wu, L. Xiao, Performance analysis of photovoltaic–thermoelectric hybrid system with and
690 without glass cover, Energy Conversion and Management 93 (2015) 151-159.
691 [35] J. Zhou, X. Zhao, X. Ma, Z. Qiu, J. Ji, Z. Du, M. Yu, Experimental investigation of a solar driven direct-
692 expansion heat pump system employing the novel PV/micro-channels-evaporator modules, Applied Energy 178
693 (2016) 484-495.
694 [36] S. Lu, R. Liang, J. Zhang, C. Zhou, Performance improvement of solar photovoltaic/thermal heat pump
695 system in winter by employing vapor injection cycle, Applied Thermal Engineering 155 (2019) 135-146.

696 [37] T.M.O. Diallo, M. Yu, J. Zhou, X. Zhao, S. Shittu, G. Li, J. Ji, D. Hardy, Energy performance analysis of a
697 novel solar PVT loop heat pipe employing a microchannel heat pipe evaporator and a PCM triple heat exchanger,
698 Energy 167 (2019) 866-888.
699 [38] H. Chen, L. Zhang, P. Jie, Y. Xiong, P. Xu, H. Zhai, Performance study of heat-pipe solar
700 photovoltaic/thermal heat pump system, Applied Energy 190 (2017) 960-980.
701 [39] X. Zhang, X. Zhao, J. Shen, J. Xu, X. Yu, Dynamic performance of a novel solar photovoltaic/loop-heat-
702 pipe heat pump system, Applied Energy 114 (2014) 335-352.
703 [40] B.J. Huang, T.H. Lin, W.C. Hung, F.S. Sun, Performance evaluation of solar photovoltaic/thermal systems,
704 Solar Energy 70(5) (2001) 443-448.
705 [41] V. Badescu, Maximum reversible work extraction from a blackbody radiation reservoir. A way to closing the
706 old controversy, EPL (Europhysics Letters) 109(4) (2015).
707 [42] V. Badescu, Unified upper bound for photothermal and photovoltaic conversion efficiency, Journal of
708 Applied Physics 103(054903) (2008).
709 [43] T.T. Chow, G. Pei, K. Fong, Z. Lin, A. Chan, J. Ji, Energy and exergy analysis of photovoltaic–thermal
710 collector with and without glass cover, Applied Energy 86(3) (2009) 310-316.
711 [44] A. Hepbasli, A key review on exergetic analysis and assessment of renewable energy resources for a
712 sustainable future, Renewable and sustainable energy reviews 12(3) (2008) 593-661.
713 [45] Z. Song, J. Ji, Y. Zhang, J. Cai, Z. Li, Y. Li, Mathematical and experimental investigation about the dual-
714 source heat pump integrating low concentrated photovoltaic and finned-tube exchanger, Energy (2022).
715